

Accelerated Article Preview**Gut-Brain Circuits for Fat Preference**

Received: 9 April 2022

Accepted: 23 August 2022

Accelerated Article Preview

Cite this article as: Li, M. et al. Gut-Brain Circuits for Fat Preference. *Nature* <https://doi.org/10.1038/s41586-022-05266-z> (2022).

Mengtong Li, Hwei-Ee Tan, Zhengyuan Lu, Katherine S. Tsang, Ashley J. Chung & Charles S. Zuker

This is a PDF file of a peer-reviewed paper that has been accepted for publication. Although unedited, the content has been subjected to preliminary formatting. Nature is providing this early version of the typeset paper as a service to our authors and readers. The text and figures will undergo copyediting and a proof review before the paper is published in its final form. Please note that during the production process errors may be discovered which could affect the content, and all legal disclaimers apply.

1 **Gut-Brain Circuits for Fat Preference**

2
3 Mengtong Li^{1,2}, Hwei-Ee Tan¹, Zhengyuan Lu^{2,3},
4 Katherine S. Tsang^{1,2}, Ashley J. Chung^{1,2} and Charles S. Zuker^{1,2,4}
5
6

7 ¹Howard Hughes Medical Institute and Department of Biochemistry and Molecular
8 Biophysics, ²Zuckerman Mind Brain and Behavior Institute, ³Department of Biological
9 Sciences and ⁴Department of Neuroscience, Vagelos College of Physicians and
10 Surgeons, Columbia University, New York, NY 10032, USA.
11

12
13 Correspondence: cz2195@columbia.edu
14

ACCELERATED ARTICLE PREVIEW

15 **Summary**

16 The perception of fat evokes strong appetitive and consummatory responses¹.
17 Here we show that fat stimuli can induce behavioural attraction even in the absence of a
18 functional taste system^{2,3}. We demonstrate that fat acts post-ingestively via the gut-
19 brain axis to drive preference for fat. Using single-cell data, we identified the vagal
20 neurons responding to intestinal delivery of fat, and showed that genetic silencing of this
21 gut-to-brain circuit abolished the development of fat preference. Next, we compared the
22 gut-to-brain pathways driving preference for fat versus sugar⁴, and uncovered two
23 parallel systems, one functioning as a general sensor of essential nutrients, responding
24 to intestinal stimulation with sugar, fat and amino acids, while the other is activated only
25 by fat stimuli. Lastly, we engineered animals lacking candidate receptors detecting the
26 presence of intestinal fat, and validated their role as the mediators of gut-to-brain fat-
27 evoked responses. Together, these findings revealed distinct cells and receptors using
28 the gut-brain axis as a fundamental conduit for the development of fat preference.

29
30
31
32
33

ACCELERATED ARTICLE PREVIEW

34 Developed and developing countries have experienced catastrophic increases in
35 the consumption of processed foods high in sugar and fat⁵. These changes in dietary
36 intake have been implicated in increases in malnutrition, including over-nutrition linked
37 to a wide number of metabolic disorders and related comorbidities^{1,6,7}.

38 Sugar and fat are essential nutrients, and consequently, animals have evolved
39 taste signalling pathways that detect and respond to sweet and fat stimuli, leading to
40 appetitive and consummatory behaviour^{1,8}. Remarkably, mice that lack sweet taste
41 receptors⁸ can still develop strong behavioural preference for sugar⁹. These results
42 suggested a taste-independent signalling pathway driving sugar preference. Indeed, we
43 recently demonstrated that the development of sugar preference is mediated by the gut
44 brain-axis, independently of the taste system⁴. Furthermore, we showed that artificial
45 sweeteners, although capable of activating the same taste receptors as sugar on the
46 tongue^{8,10}, do not activate the gut-brain sugar circuit, and consequently do not create a
47 preference⁴. Together, these findings revealed a gut-to-brain, post-ingestive intestinal
48 sugar-sensing pathway, driving craving and attraction to sugar^{4,11-14}.

49 Here we focus our attention on the neural basis of fat preference. We
50 demonstrate that fat, like sugar, uses the gut-brain axis to drive consumption. Then, we
51 dissect the nature of the receptors and neuronal elements mediating the development of
52 fat preference.

53 The discovery of post-ingestive mechanisms activated by foods rich in sugar and
54 fat can provide valuable strategies to modulate our sugar- and fat-craving eating habits,
55 and help combat obesity and associated disorders, including diabetes and
56 cardiovascular disease.

57

58 **The development of fat preference**

59 To behaviourally monitor the development of post-ingestive fat preference, we
60 presented animals with a choice between an artificial sweetener (3 mM acesulfame K,
61 AceK) and fat (1.5% Intralipid, IL) (Fig. 1a). While both stimuli are innately attractive to a
62 naive animal^{8,15} (see Extended Data Fig. 1a, b), artificial sweeteners do not trigger post-
63 oral preference^{4,16}. Therefore, this fat versus sweetener test allows us to monitor the
64 emergence of fat preference, from an initial state of no-preference to its switch into a

65 strongly appetitive stimuli. Indeed, our results showed that, although animals initially
66 preferred the artificial sweetener (Fig. 1a, b “Pre”), within 24 h of exposure to both
67 choices, their preference is markedly altered, such that by 48 h, the mice drink almost
68 exclusively from the bottle containing fat (Fig. 1a, b “Post”). This behavioural switch
69 illustrates the ability of fat stimuli to post-ingestively induce strong consummatory
70 responses and appetitive behaviour¹. This switch is also observed when comparing fat
71 to an equicaloric sugar (Extended Data Fig. 1e, f), showing that calories are not driving
72 the development of fat preference.

73 Recently, it was shown that the immediate attraction to fat is dependent on the
74 TRPM5 channel expressed in taste receptor cells³ (Extended Data Fig. 1c). We
75 hypothesized that if the development of fat preference is mediated via post-ingestive,
76 rather than taste-evoked signalling, it should be independent of TRPM5 function, and
77 consequently TRPM5 knockout animals should still be capable of developing
78 behavioural preference for fat. As predicted, TRPM5 mutant animals, while blind to the
79 taste of fat, still are fully capable of developing strong post-ingestive preference for fat³
80 (Extended Data Fig. 1d).

81

82 **Fat preference via the gut-brain axis**

83 For an animal to develop a preference for fat over sweetener, it must distinguish
84 between two innately attractive stimuli. We reasoned that if we could identify a
85 population of brain neurons that respond selectively to the consumption of fat, it may
86 provide an entry to reveal the neural control of fat preference and the basis for the
87 insatiable appetite for fat.

88 We exposed separate cohorts of animals to three different lipid stimuli (Intralipid,
89 linoleic acid, or oleic acid) and to fat-free textural controls (xanthan gum or mineral oil).
90 Using Fos as a proxy for neural activity^{4,17}, we found that fat, but not control
91 stimuli, elicited strong bilateral activation of neurons in the caudal nucleus of the solitary
92 tract (cNST) in the brainstem (Fig. 1c, d, Extended Data Fig. 2a-e). The cNST is a
93 nexus of interoceptive signals conveying information from the body to the brain via the
94 gut-brain axis^{18,19}. If the fat-activated brain cNST neurons are receiving signals
95 originating in the gut, then direct delivery of fat stimuli into the gut should also induce

96 activation of the cNST. We implanted an intragastric catheter in the stomach⁴ and
97 infused either a fat solution or a vehicle control. As predicted, intragastric infusion of fat,
98 but not of a vehicle, is also sufficient to activate the cNST (Extended Data Fig. 2j-l).

99 Next, we reasoned that if the fat-activated cNST neurons are essential for
100 creating fat preference, then blocking their function should prevent the development of
101 fat preference. We used the targeted recombination in active populations (TRAP)²⁰
102 system to target Cre recombinase to fat-activated cNST neurons, and bilaterally injected
103 an adeno-associated virus (AAV) carrying a Cre-dependent tetanus toxin light chain
104 (TetTox)²¹ construct, so as to genetically silence synaptic transmission in the cNST
105 neurons responding to fat (Fig. 2a, Extended Data Fig. 3).

106 To ensure that the genetic silencing did not affect the animals' immediate
107 attraction to fat (i.e. the taste-dependent innate attraction), they were first tested in a
108 standard fat versus water two-bottle discrimination assay. Our results showed that the
109 silenced mice still exhibit normal immediate attraction to fat, and were indistinguishable
110 from controls (Extended Data Fig. 2f-i). By contrast, they were unable to develop post-
111 ingestive preference for fat, even after prolonged testing sessions (Fig. 2a).

112

113 **Fat and sugar activated vagal neurons**

114 To investigate how fat signals are transferred from the gut to the brain, we
115 infused fat stimuli into the gut, and used fibre photometry to simultaneously record
116 neural activity in cNST neurons⁴ (Fig. 2b). Our results showed that cNST neurons are
117 robustly activated by direct intestinal infusion of fat, with responses tracking the delivery
118 of the stimulus (Fig. 2c, d, Extended Data Fig. 3f-i).

119 We and others have shown that the vagus nerve serves as a key conduit for
120 conveying information from the gut to the brain^{4,12,13,19,22}. If the vagus nerve is required
121 for the transmission of fat signals from the gut to the cNST, then transection of the
122 vagus nerve should prevent the signals from reaching the brain. To test this hypothesis,
123 we infused the gut with fat (or sugar as a control⁴) and recorded stimulus-evoked
124 responses in the cNST. Indeed, fat-activated neural responses in the cNST were
125 effectively abolished after bilateral vagotomy (Fig. 2c, d, Extended Data Fig. 3f-i), thus

126 establishing the vagus nerve as the conduit for transmitting the fat signal from the gut to
127 the brain.

128 To directly examine, and monitor the fat responses of vagal sensory neurons, we
129 carried out functional imaging of the nodose ganglion (which contains the cell bodies of
130 vagal neurons). We targeted the genetically encoded calcium indicator GCaMP6s²³ to
131 vagal sensory neurons using *Vglut2-Cre* animals^{4,24,25}, and used a one-photon calcium
132 imaging set-up coupled to synchronous intestinal delivery of fat to record neuronal
133 responses *in vivo*⁴, with real time kinetics (Fig. 2e, Extended Data Fig. 4a-c). To
134 administer the stimuli, a catheter was placed into the duodenal bulb, and an exit port
135 was created by transecting the intestine 10 cm distally. During each imaging session,
136 the intestine was exposed to a pre-stimulus application of PBS, a 10 s (33 ul) exposure
137 to the fat or sugar stimuli, and a 180 s post-stimulus wash (see Methods for details); this
138 regime was repeated at least 3 times for each stimulus. Using this preparation, we
139 showed that intestinal infusion of fat (e.g. linoleic acid), but not vehicle control, evoked
140 robust responses in a unique subset of vagal neurons (Fig. 2e, Extended Data Fig. 4c,
141 d); the responses were reproducible and time-locked to stimulus delivery (Fig. 2e,
142 Extended Data Fig. 4c). These neurons responded to a variety of dietary fatty acids
143 (Extended Data Fig. 4d-i), thus defining a distinct class of vagal neurons reliably
144 activated by intestinal fat stimuli.

145 Previously, we showed that intestinal application of glucose also activates a
146 subset of vagal neurons⁴, and demonstrated that these, in turn, are part of the essential
147 gut-brain axis driving the development of sugar preference. Next, we sought to examine
148 how vagal neurons respond to these two nutrient signals in the gut: fat and sugar.

149 We recorded the activity of vagal neurons to alternating gut stimulation with fat
150 and sugar (10 s of 10% linoleic acid and 10 s of 500 mM glucose). Remarkably, from
151 over 1800 vagal sensory neurons examined from 22 nodoses, we identified two distinct
152 groups of vagal neurons. One group (~8% of the total imaged neurons) responded to
153 both sugar and fat. The other, a non-overlapping group (also ~8% of the neurons),
154 responded only to fat, but not to sugar (Fig. 2f, Extended Data Fig. 5a). Notably, the
155 subset responding to sugar and fat was also activated by amino acids (Fig. 3a,
156 Extended Data Fig. 5b, c). These results defined two distinct populations of vagal

157 neurons: one, hereafter referred to as sugar/fat responders, function as sensors for all
158 three essential macronutrients in the gut: sugar, proteins and fat. The other, herein
159 referred to as fat-only, responds selectively to intestinal delivery of fat. We note that less
160 than one neuron per nodose was found to respond to intestinal delivery of sugar or
161 amino acids but not fat (Extended Data Fig. 5d), however, given such small numbers,
162 these were not considered further (it is likely they represent sugar/nutrient responders
163 with very small responses to fat).

164

165 **Fat and sugar signalling in the gut**

166 How are sugar/nutrient signals transmitted from the gut to vagal neurons? The
167 cholecystokinin (CCK)-expressing enteroendocrine cells (EECs) in the intestines have
168 been proposed to function as the sugar-preference gut sensing cells^{11,26}. We
169 hypothesized that CCK may be the signal between the gut and their partner vagal
170 neurons. Hence, we examined responses of vagal neurons to intestinal application of
171 sugar, fat and amino acids, before and after pharmacologically inhibiting CCK signalling
172 with Devazepide²⁷, a CCK-A receptor²⁸ (CCKAR) antagonist (Fig. 3a). Indeed, blocking
173 CCK signalling abolished all the responses of the vagal sugar/fat neurons (i.e. to
174 intestinal stimulation with sugar, fat and amino acids). In contrast, the fat-only
175 responses remained robust and reliable (Fig. 3a, b, Extended Data Fig. 6). Given these
176 results, we anticipated that application of CCK should strongly activate the nutrient
177 responding vagal neurons, but not the fat-only neurons. Our results proved both
178 predictions to be correct (Extended Data Fig. 6f). Finally, we also examined the
179 potential role of glutamate signalling¹¹ by imaging responses of vagal neurons to
180 intestinal sugar stimuli before and after addition of a mixture of L-(+)-2-Amino-3-
181 phosphonopropionic acid (AP3) and kynurenic acid (KA), two glutamate receptor
182 antagonists^{29,30}. Our results demonstrated that pharmacological inhibition of glutamate-
183 based signalling has no effect on the gut-to-vagal sugar/nutrient sensing circuit
184 (Extended Data Fig. 6a-d). Together, these results substantiate CCK as the transmitter
185 mediating sugar/nutrient sensing in the gut-brain axis, and further distinguishes the
186 CCK-dependent, from the CCK-independent fat-sensing gut-to-brain pathways.

187

188 **Nutrient responders in the nodose**

189 Given that gut sugar/fat/amino acid responders rely on CCK signalling, we
190 expected that vagal neurons receiving this gut-to-brain signal should be defined by
191 expression of CCK receptors (e.g. CCKAR; Fig. 3c). CCK is principally known as a
192 satiety hormone, whose role is to modulate food intake by suppressing appetite^{31,32}. The
193 function of nutrient preference circuits, on the other hand, is to promote nutrient
194 consumption^{1,4}. Thus, we wondered how CCK can function both as a satiety hormone
195 and as a nutrient preference signal in the gut. We reasoned this conundrum could be
196 easily resolved if a genetically distinct³³ subset of CCKAR-expressing vagal neurons
197 mediates nutrient preference.

198 First, we engineered *Cckar-Cre* mice by targeting Cre recombinase to the CCK-
199 receptor A gene³⁴ (see Methods), and used them to functionally validate the nutrient-
200 evoked activation of CCKAR-vagal neurons (Extended Data Fig. 7a, b). Next, we used
201 single-cell RNA-seq data from the nodose ganglion³⁵⁻³⁷ to further characterize subsets
202 of CCKAR-expressing neurons, and generated Cre driver lines expressing GCaMP6s in
203 subsets of candidate clusters. Our results showed that a unique pool of CCKAR-
204 expressing vagal neurons, marked by expression of the vasoactive intestinal peptide
205 (VIP), labeled the nutrient responders (with only a small fraction of the fat-only neurons)
206 (Fig. 3c, d, Extended Data Fig. 7e-g). We then further refined this cluster by removing
207 the small number of fat-only responding neurons (Extended Data Fig. 7c, d, g). These
208 results validate the segregation of the nutrient versus the fat-only circuit, and
209 substantiate CCK in the gut as the transmitter mediating sugar/nutrient signals.

210 An important prediction is that inhibiting signalling from the nutrient-sensing vagal
211 neurons should prevent the activation of the gut-brain axis, and consequently block the
212 development of nutrient preference. Our strategy was to genetically silence the nutrient
213 sensing vagal neurons by bilaterally injecting the nodose of *Vip-Cre*³⁸ mice with an AAV-
214 Flex-TetTox⁴ construct (Fig. 4a, Extended Data Fig. 3d). As hypothesized, blocking
215 activity from these neurons dramatically impaired the development of nutrient
216 preference (Fig. 4b, c). Importantly, the immediate, innate attraction to sugar and fat in
217 these animals was not affected (Extended Data Fig. 8).

218 Finally, we anticipated that artificial activation of this gut-to-brain nutrient
219 preference circuit should afford the development of new preferences, in essence driving
220 appetitive responses to previously unpreferred stimuli. To test this proposal, we
221 bilaterally injected the nodose of *Vip-Cre* mice with a Cre-dependent AAV virus
222 encoding the excitatory designer receptor hM3Dq³⁹, such that nutrient responding
223 neurons could be experimentally activated by the DREADD agonist clozapine⁴⁰. After
224 allowing expression of DREADD (Extended Data Fig. 3e), animals were exposed to a
225 preference assay using cherry- versus a grape-flavoured solution (Fig. 4d), and to
226 enhance attraction of these novel flavours, both solutions were spiked with an artificial
227 sweetener (see Methods). Next, we established a baseline preference for each animal
228 (i.e. grape vs cherry), introduced clozapine into the less-preferred flavour, and
229 investigated whether clozapine-mediated activation of the nutrient sensing neurons can
230 create a new preference. Indeed, after 48 h of exposure to both solutions all of the
231 animals markedly switched their preference to the clozapine containing flavour. By
232 contrast, mice without the designer receptor did not develop a new preference, and if
233 anything, were slightly averse to the DREADD activator (Fig. 4e). These results
234 illustrate how non-natural activation of this gut-brain sugar/nutrient sensing circuit can
235 drive the development of a novel preference.

236

237 **Fat-only responders in the nodose**

238 What about the identity of vagal neurons mediating the fat-only signals? Using
239 the single-cell RNA-seq atlas from the nodose ganglion³⁵⁻³⁷, we searched for vagal
240 neurons that did not express VIP (as the sugar/fat/amino acid sensing marker), and
241 identified 5 minimally overlapping candidate clusters (Fig. 5a): *Trpa1* (transient receptor
242 potential ankyrin 1), *Gpr65* (G Protein-Coupled Receptor 65), *Piezo2* (Piezo Type
243 Mechanosensitive Ion Channel Component 2), *Calca* (Calcitonin Related Polypeptide
244 Alpha), and *Oxtr* (Oxytocin Receptor). We engineered *Trpa1-Cre* mice using the
245 CRISPR/Cas9 system (Extended Data Fig. 9a, and also see Methods), and obtained
246 Cre driver lines for the other 4 candidates. Our results (Fig. 5b), demonstrated that the
247 TRPA1-expressing vagal cluster selectively responds to intestinal delivery of fat, but not
248 sugar or amino acid stimuli, thus defining the fat-only responders. Vagal neurons

249 expressing GCaMP6s in *Gpr65-Cre*, *Piezo2-Cre*, *Calca-Cre*, or *Oxtr-Cre* were
250 unresponsive to intestinal delivery of sugar or fat stimuli (Extended Data Fig. 9b-e).

251 Next, we reasoned that genetic silencing of the fat-only circuit (i.e. TRPA1-
252 expressing vagal neurons) may abolish the development of fat preference, but should
253 have no impact on the development of sugar preference. Thus, we bilaterally injected
254 the nodose of *Trpa1-Cre* mice with an AAV-Flex-TetTox construct to silence the fat-only
255 vagal neurons, and tested the animals for sugar- versus fat preference. Indeed, after
256 genetic silencing, these mice can no longer develop post-ingestive preference for fat
257 stimuli, but retain their capacity to develop post-ingestive preference for sugar (Fig. 5c).
258 Importantly, their immediate attraction to fat is unaffected (Extended Data Fig. 8)
259 Together, these results reveal the identity of the neurons mediating fat-only signals, and
260 uncover their essential role in the gut-to-brain circuit mediating fat preference (see
261 discussion).

262

263 **Sugar and fat sensors in the gut**

264 Previously, we used pharmacological experiments to demonstrate that the
265 sodium–glucose-linked transporter-1 (SGLT1) functions as the gut receptor recognizing
266 glucose and transmitting the post-ingestive⁴¹, gut-to-brain sugar signals⁴. Here, we
267 extend the specificity of these findings by generating SGLT1 knockout animals and
268 examining their responses to intestinal stimulation with sugar and fat (Fig. 6a). The data
269 shown in Figure 6 demonstrates that all vagal responses to intestinal delivery of sugar
270 are abolished. In contrast, responses to fat stimuli are unaffected.

271 We expected that the development of fat preference should depend on specific
272 fat receptors expressed on the surface of intestinal EECs⁴². Dietary fat, once ingested
273 and digested, is thought to be sensed by a number of putative gut receptors, including
274 the fatty acid translocase CD36^{43,44} and the G protein-coupled receptors GPR40⁴⁵ and
275 GPR120^{46,47}. We anticipated that one or more of these receptors may be used to
276 transmit fat preference⁴⁶ via the gut-brain axis. Therefore, we used CRISPR-Cas9 to
277 generate animals harbouring knockouts of CD36, GPR40, and GPR120 in all possible
278 knockout combinations (single, double, and triple mutants, Extended Data Fig. 9f; see
279 Methods for details).

280 A key prediction would be that loss of the essential receptor(s) should abolish
281 vagal responses to intestinal stimulation with fat, thus defining the intestinal sensors for
282 the gut-to-brain fat signals.

283 Because of the intricacies of breeding such a wide range of knockout
284 combinations, and the need to introduce the GCaMP6s reporter for functional imaging
285 into the various genetic backgrounds, we chose to use a direct fusion of GCaMP6s to
286 Snap25 regulatory sequences⁴⁸ rather than crossing-in a Cre-driver construct and a
287 Cre-dependent GCaMP reporter. Our results showed that the Snap25-GCaMP6s
288 construct is well expressed in vagal neurons, and compares favourably with our studies
289 using other driver lines (Extended Data Fig. 9g, h).

290 After testing all the fat receptor-deletion combinations (Fig. 6c, d, Extended Data
291 Fig. 10a-f), we found that GPR40 and GPR120 are the essential mediators of intestinal
292 fat signals to the vagal neurons. As expected, vagal neurons responding to sugar were
293 unaffected in all of the mutant combinations (Extended Data Fig. 10a-g). Importantly, all
294 fat responses, from both the fat-only and from the sugar/fat/amino acid sensing vagal
295 neurons, were abolished in the GPR40/GPR120 knockout animals, demonstrating that
296 the same receptors are used in both gut-to-brain signalling pathways (i.e. CCK-
297 independent and CCK-dependent, respectively).

298 An expectation from these imaging results is that GPR40/GPR120 double
299 knockout animals (as well as the triple knockout) should fail to develop preference for
300 fat⁴⁶, while the various single and other double mutants should be unaffected. We note,
301 however, that these are global knockouts, rather than conditional knockouts. Notably,
302 GPR40, GPR120 and CD36 single mutants, as well as GPR40/CD36 and
303 GPR120/CD36 double mutants are indistinguishable from control wild type mice (Fig.
304 6e, right panel). By contrast, the GPR40/GPR120 double (and the triple mutants) are no
305 longer capable of developing behavioural preference for fat (Fig. 6e, left panel).

306 Significantly, the innate responses to fat stimuli were unaffected in the GPR40/GPR120
307 double and triple mutants, with the animals exhibiting strong immediate attraction to fat,
308 illustrating the fundamental difference between the taste and the gut-brain pathways
309 (Extended Data Fig. 10h). Just like control mice, fat receptor knockouts develop normal
310 preference for sugar⁴⁶ (Fig. 6f). Together, these results substantiate GPR40 and

311 GPR120 as the essential receptors signalling the presence of intestinal fat via the gut-
312 brain axis.

313

314 **Discussion**

315 Sugar and fat are indispensable nutrients, and it would be expected that
316 dedicated circuits drive their consumption^{1,4,13}. We have shown that in addition to the
317 taste system, these nutrients rely on a dedicated gut-to-brain system to detect and
318 report the presence of intestinal sugar and fat to the brain.

319 Here, we demonstrate the fundamental role of these nutrient-sensing circuits by
320 showing that genetic or pharmacological blockade of sugar and fat gut-to-brain signals,
321 at any of the 4 stages following ingestion, abolished the development of nutrient
322 preference: (1) by preventing sugar or fat binding to their corresponding intestinal
323 receptors, (2) by blocking the activated gut cells from signaling to the vagal neurons, (3)
324 by silencing the sugar- or fat-activated vagal neurons, and preventing the transfer of
325 their signals to the brain, and (4) finally, by preventing the cNST neurons that receive
326 the gut-brain signals from broadcasting the presence of intestinal sugar or fat to the rest
327 of the brain.

328 An unexpected finding from these studies was the discovery of a single gut-to-
329 brain pathway, based on CCK signalling, that functions as a generalist detector
330 informing the brain of the intestinal presence of any of the three essential nutrients:
331 sugar, fat and amino acids. Although each nutrient uses its own dedicated receptors in
332 the gut, the convergence of the signal into a unique class of vagal neurons (VIP/UTS2b)
333 highlights the simple and elegant logic of this circuit: after the gut cells are activated, the
334 circuit does not need to preserve the identity of the specific nutrient stimulus, only to
335 ensure that the emerging gut-brain message signal trigger behavioral preference⁴.
336 Given that CCK functions as the signalling molecule in the gut for the sugar/nutrient
337 sensing pathway, we anticipate that there would be a unique subset of intestinal CCK-
338 positive EECs that co-express the sugar (SGLT1) and the fat (GPR40 and GPR120)
339 preference receptors (the nature of the amino acid receptor is not yet known).
340 Interestingly, examination of single-cell RNA atlases from both rodent and human gut
341 tissue suggests this is likely the case^{33,49}. Future studies should help define this

342 subtype of CCK enteroendocrine cell that uses CCK as a transmitter (rather than as a
343 gut neuromodulator or hormone) to activate the gut-brain axis, and report the presence
344 of intestinal sugar, fat and amino acid nutrients.

345 Our results also uncovered two separate gut-brain circuits for intestinal fat
346 sensing (i.e. the fat-only and the sugar/fat/amino acid vagal pathways), yet both utilize
347 the same receptors, GPR40 and GPR120, for driving the development of fat preference.
348 Surprisingly, silencing either circuit is sufficient to abolish preference for fat,
349 demonstrating that both are indispensable for the development of fat preference. Thus,
350 activating the fat intestinal receptors only in the CCK-dependent pathway, or only in the
351 CCK-independent (fat-only) pathway, is not sufficient on their own to trigger fat
352 preference. Indeed, we measured cNST signals activated solely by the fat-only
353 pathway, and they are about 50% of the signal detected when both fat preference
354 pathways are active (see Extended Data Fig. 6g-i).

355 Given the essential role of sugar and fat in a healthy diet, and the importance of
356 these gut-brain pathways in sugar and fat consumption (and most likely over-
357 consumption), it will be of great interest to determine the brain targets for each, and
358 compare and contrast their logic.

359 Finally, the identification of these gut receptors and gut-brain communication
360 lines could help provide novel strategies to moderate the insatiable appetite for fat and
361 sugar. Additionally, they clarify the fundamental difference between “liking” and
362 “wanting”⁵⁰. Liking sweet and liking fat (i.e. the innate attraction to these appetitive
363 stimuli), is the result of activation of the taste system. Wanting sugar and fat, on the
364 other hand, is the gut-brain axis.

365

366

367

368

369

370

371

372

373 **References**

374

- 375 1. Berthoud, H. R., Morrison, C. D., Ackroff, K. & Sclafani, A. Learning of food
376 preferences: mechanisms and implications for obesity & metabolic diseases. *Int J*
377 *Obes (Lond)* **45**, 2156-2168, (2021).
- 378 2. Zhang, Y. *et al.* Coding of sweet, bitter, and umami tastes: different receptor cells
379 sharing similar signaling pathways. *Cell* **112**, 293-301, (2003).
- 380 3. Sclafani, A. & Ackroff, K. Fat preference deficits and experience-induced
381 recovery in global taste-deficient Trpm5 and Calhm1 knockout mice. *Physiol*
382 *Behav* **246**, 113695, (2022).
- 383 4. Tan, H. E. *et al.* The gut-brain axis mediates sugar preference. *Nature* **580**, 511-
384 516, (2020).
- 385 5. *Food and Agriculture Organization of the United Nations (FAO)*
386 <https://www.fao.org/faostat/en/#data/FBS> (2020).
- 387 6. Hu, F. B., van Dam, R. M. & Liu, S. Diet and risk of Type II diabetes: the role of
388 types of fat and carbohydrate. *Diabetologia* **44**, 805-817, (2001).
- 389 7. Smilowitz, J. T., German, J. B. & Zivkovic, A. M. Food Intake and Obesity: The
390 Case of Fat. *Frontiers in Neuroscience* (eds J. P. Montmayeur & J. le Coutre)
391 (2010).
- 392 8. Zhao, G. Q. *et al.* The receptors for mammalian sweet and umami taste. *Cell*
393 **115**, 255-266, (2003).
- 394 9. Sclafani, A., Marambaud, P. & Ackroff, K. Sucrose-conditioned flavor preferences
395 in sweet ageusic T1r3 and Calhm1 knockout mice. *Physiol Behav* **126**, 25-29,
396 (2014).
- 397 10. Nelson, G. *et al.* Mammalian sweet taste receptors. *Cell* **106**, 381-390, (2001).
- 398 11. Buchanan, K. L. *et al.* The preference for sugar over sweetener depends on a gut
399 sensor cell. *Nat Neurosci* **25**, 191-200, (2022).
- 400 12. Han, W. *et al.* A Neural Circuit for Gut-Induced Reward. *Cell* **175**, 887-888,
401 (2018).
- 402 13. Goldstein, N. *et al.* Hypothalamic detection of macronutrients via multiple gut-
403 brain pathways. *Cell Metab* **33**, 676-687 e675, (2021).

- 404 14. Su, Z., Alhadeff, A. L. & Betley, J. N. Nutritive, Post-ingestive Signals Are the
405 Primary Regulators of AgRP Neuron Activity. *Cell Rep* **21**, 2724-2736, (2017).
- 406 15. Yoneda, T. *et al.* The palatability of corn oil and linoleic acid to mice as measured
407 by short-term two-bottle choice and licking tests. *Physiol Behav* **91**, 304-309,
408 (2007).
- 409 16. Sclafani, A., Zukerman, S. & Ackroff, K. Postoral glucose sensing, not caloric
410 content, determines sugar reward in C57BL/6J mice. *Chem Senses* **40**, 245-258,
411 (2015).
- 412 17. Sheng, M. & Greenberg, M. E. The regulation and function of c-fos and other
413 immediate early genes in the nervous system. *Neuron* **4**, 477-485, (1990).
- 414 18. Berthoud, H. R. & Neuhuber, W. L. Functional and chemical anatomy of the
415 afferent vagal system. *Auton Neurosci* **85**, 1-17, (2000).
- 416 19. Prescott, S. L. & Liberles, S. D. Internal senses of the vagus nerve. *Neuron*,
417 (2022).
- 418 20. Guenther, C. J., Miyamichi, K., Yang, H. H., Heller, H. C. & Luo, L. Permanent
419 genetic access to transiently active neurons via TRAP: targeted recombination in
420 active populations. *Neuron* **78**, 773-784, (2013).
- 421 21. Yamamoto, M. *et al.* Reversible suppression of glutamatergic neurotransmission
422 of cerebellar granule cells in vivo by genetically manipulated expression of
423 tetanus neurotoxin light chain. *J Neurosci* **23**, 6759-6767, (2003).
- 424 22. Williams, E. K. *et al.* Sensory Neurons that Detect Stretch and Nutrients in the
425 Digestive System. *Cell* **166**, 209-221, (2016).
- 426 23. Chen, T. W. *et al.* Ultrasensitive fluorescent proteins for imaging neuronal
427 activity. *Nature* **499**, 295-300, (2013).
- 428 24. Chang, R. B., Strohlic, D. E., Williams, E. K., Umans, B. D. & Liberles, S. D.
429 Vagal Sensory Neuron Subtypes that Differentially Control Breathing. *Cell* **161**,
430 622-633, (2015).
- 431 25. Raab, M. & Neuhuber, W. L. Glutamatergic functions of primary afferent neurons
432 with special emphasis on vagal afferents. *Int Rev Cytol* **256**, 223-275, (2007).
- 433 26. Kaelberer, M. M. *et al.* A gut-brain neural circuit for nutrient sensory transduction.
434 *Science* **361**, (2018).

- 435 27. Chang, R. S. & Lotti, V. J. Biochemical and pharmacological characterization of
436 an extremely potent and selective nonpeptide cholecystokinin antagonist. *Proc*
437 *Natl Acad Sci U S A* **83**, 4923-4926, (1986).
- 438 28. Dufresne, M., Seva, C. & Fourmy, D. Cholecystokinin and gastrin receptors.
439 *Physiol Rev* **86**, 805-847, (2006).
- 440 29. Hansen, K. B. *et al.* Structure, Function, and Pharmacology of Glutamate
441 Receptor Ion Channels. *Pharmacol Rev* **73**, 298-487, (2021).
- 442 30. Niswender, C. M. & Conn, P. J. Metabotropic glutamate receptors: physiology,
443 pharmacology, and disease. *Annu Rev Pharmacol Toxicol* **50**, 295-322, (2010).
- 444 31. Gibbs, J., Young, R. C. & Smith, G. P. Cholecystokinin decreases food intake in
445 rats. *J Comp Physiol Psychol* **84**, 488-495, (1973).
- 446 32. Liddle, R. A. Cholecystokinin cells. *Annu Rev Physiol* **59**, 221-242, (1997).
- 447 33. Bai, L. *et al.* Enteroendocrine cell types that drive food reward and aversion.
448 *bioRxiv*, (2021).
- 449 34. Lacourse, K. A., Lay, J. M., Swanberg, L. J., Jenkins, C. & Samuelson, L. C.
450 Molecular structure of the mouse CCK-A receptor gene. *Biochem Biophys Res*
451 *Commun* **236**, 630-635, (1997).
- 452 35. Kupari, J., Haring, M., Agirre, E., Castelo-Branco, G. & Ernfors, P. An Atlas of
453 Vagal Sensory Neurons and Their Molecular Specialization. *Cell Rep* **27**, 2508-
454 2523 e2504, (2019).
- 455 36. Prescott, S. L., Umans, B. D., Williams, E. K., Brust, R. D. & Liberles, S. D. An
456 Airway Protection Program Revealed by Sweeping Genetic Control of Vagal
457 Afferents. *Cell* **181**, 574-589 e514, (2020).
- 458 37. Bai, L. *et al.* Genetic Identification of Vagal Sensory Neurons That Control
459 Feeding. *Cell* **179**, 1129-1143 e1123, (2019).
- 460 38. Taniguchi, H. *et al.* A resource of Cre driver lines for genetic targeting of
461 GABAergic neurons in cerebral cortex. *Neuron* **71**, 995-1013, (2011).
- 462 39. Armbruster, B. N., Li, X., Pausch, M. H., Herlitze, S. & Roth, B. L. Evolving the
463 lock to fit the key to create a family of G protein-coupled receptors potently
464 activated by an inert ligand. *Proc Natl Acad Sci U S A* **104**, 5163-5168, (2007).

- 465 40. Gomez, J. L. *et al.* Chemogenetics revealed: DREADD occupancy and activation
466 via converted clozapine. *Science* **357**, 503-507, (2017).
- 467 41. Sclafani, A., Koepsell, H. & Ackroff, K. SGLT1 sugar transporter/sensor is
468 required for post-oral glucose appetition. *Am J Physiol Regul Integr Comp*
469 *Physiol* **310**, R631-639, (2016).
- 470 42. Gribble, F. M. & Reimann, F. Enteroendocrine Cells: Chemosensors in the
471 Intestinal Epithelium. *Annu Rev Physiol* **78**, 277-299, (2016).
- 472 43. Schwartz, G. J. *et al.* The lipid messenger OEA links dietary fat intake to satiety.
473 *Cell Metab* **8**, 281-288, (2008).
- 474 44. Pepino, M. Y., Kuda, O., Samovski, D. & Abumrad, N. A. Structure-function of
475 CD36 and importance of fatty acid signal transduction in fat metabolism. *Annu*
476 *Rev Nutr* **34**, 281-303, (2014).
- 477 45. Edfalk, S., Steneberg, P. & Edlund, H. Gpr40 is expressed in enteroendocrine
478 cells and mediates free fatty acid stimulation of incretin secretion. *Diabetes* **57**,
479 2280-2287, (2008).
- 480 46. Sclafani, A., Zukerman, S. & Ackroff, K. GPR40 and GPR120 fatty acid sensors
481 are critical for postoral but not oral mediation of fat preferences in the mouse. *Am*
482 *J Physiol Regul Integr Comp Physiol* **305**, R1490-1497, (2013).
- 483 47. Hirasawa, A. *et al.* Free fatty acids regulate gut incretin glucagon-like peptide-1
484 secretion through GPR120. *Nat Med* **11**, 90-94, (2005).
- 485 48. Madisen, L. *et al.* Transgenic mice for intersectional targeting of neural sensors
486 and effectors with high specificity and performance. *Neuron* **85**, 942-958, (2015).
- 487 49. Haber, A. L. *et al.* A single-cell survey of the small intestinal epithelium. *Nature*
488 **551**, 333-339, (2017).
- 489 50. de Araujo, I. E., Schatzker, M. & Small, D. M. Rethinking Food Reward. *Annu*
490 *Rev Psychol* **71**, 139-164, (2020).

491
492
493
494
495

496 **Figure legends**

497

498 **Figure 1: The development of fat preference**

499 **a**, Cartoon on the left illustrates the behavioural arena; mice were allowed to
500 choose between a fat emulsion (1.5% Intralipid, IL) and an artificial sweetener (3mM
501 AceK). Preference was tracked by electronic lick counters in each port. The graph
502 shows cumulative licks for each bottle over the 48 h session. The colour bars at the top
503 show lick rasters for fat (red) and sweet (blue) from the first and last 2000 licks of the
504 behavioural test. Note that by 24 h the animals begin to drink almost exclusively from
505 the fat bottle (red trace). **b**, Preference plots for fat versus sweet. In these experiments,
506 mice began the preference test preferring sweet (preference index < 0.5), but in all
507 cases they switched their preference to fat ($n=7$ mice, two-tailed paired t-test, $P=1.9 \times 10^{-5}$). **c**, Schematic of fat stimulation of Fos induction. Strong Fos labelling is observed in
509 the cNST (highlighted yellow) upon ingestion of Intralipid (20%) but not control stimuli
510 (0.3% xanthan gum). Scale bars, 100 μm . **d**, Quantification of Fos-positive neurons. The
511 equivalent area of the cNST (200 μm x 200 μm ; Bregma -7.5 mm) was processed, and
512 positive neurons were counted for the different stimuli. Two-sided Mann–Whitney U-test
513 between xanthan gum (XG) and Intralipid (IL) ($n=5$ mice), $P=7.9 \times 10^{-3}$. Values are mean
514 \pm s.e.m.

515

516 **Figure 2: Fat preference is mediated by the gut-brain axis**

517 **a**, Left panel: Schematic for silencing fat-stimulated cNST neurons. A TetTox
518 virus was targeted bilaterally to the cNST of TRAP2 mice for silencing. Right Panel: The
519 bars graphs show the fraction of Acek versus Intralipid (IL) consumption, after the 48 h
520 preference test, in control ($n=10$) versus TetTox mice ($n=9$). Two-sided Mann–Whitney
521 U-test for fat, $P=1.4 \times 10^{-3}$ (total volume consumed: control 9.9 ± 2.3 ml, TetTox 8.3 ± 2.1
522 ml). Control animals developed a strong preference for Intralipid versus sweetener. In
523 contrast, animals in which fat-activated cNST neurons were silenced no longer exhibit a
524 preference for fat over sweetener. Values are mean \pm s.e.m. **b**, Fiber photometry was
525 used to monitor activity in cNST neurons in response to intestinal delivery of fat. **c**,
526 Neural responses following 10 s intestinal delivery of fat (10% linoleic acid, LA) or

527 control sugar (500mM glucose, Glu). The solid trace is the average and the shaded
528 area represents s.e.m. Responses after bilateral vagotomy are shown in green. $n=6$
529 mice. NR, normalized response. Note total loss of responses following bilateral
530 vagotomy⁴. **d**, Quantification of neural responses pre- and post-vagotomy. Two-tailed
531 paired t-test, $P=4.6 \times 10^{-8}$ (sugar), $P=4.9 \times 10^{-8}$ (fat). Values are mean \pm s.e.m. **e**, Imaging
532 of calcium responses in vagal neurons while delivering stimuli into the intestines. Heat
533 maps depict z-score-normalized fluorescence traces from vagal neurons identified as fat
534 responders ($n=84/515$ cells from 8 ganglia). Each row represents the average activity of
535 a single cell to four trials. Stimulus window (10 s) is shown by dotted white lines. Note
536 strong responses to intestinal delivery of fat but not to control stimuli. Control, 0.1%
537 xanthan gum plus 0.05% Tween 80; fat, 10% linoleic acid (LA). Shown below are
538 sample traces of responses to alternating 10 s pulses of control (XG) and fat stimuli
539 (LA). **f**, Heat maps depict z-score-normalized responses to interleaved 10 s stimuli of
540 fat (10% linoleic acid, LA) and sugar (500mM glucose, Glu). Each row represents the
541 average activity of a different neuron during three exposures to the stimulus. The upper
542 panels show 151 neurons that responded to intestinal application of both fat and
543 glucose. The bottom panel shows a different pool of 153 neurons that responded only to
544 fat. $n=22$ vagal ganglia, 1813 neurons were imaged.

545

546 **Figure 3: Nutrients engage gut-to-vagal CCK-mediated signaling**

547 **a**, Imaging of calcium responses in vagal sensory neurons⁴ while delivering fat,
548 sugar, or amino acid stimuli into the intestines (10% linoleic acid, 500mM glucose or a
549 250mM amino acid mixture; see Methods). Heat maps depict z-score-normalized
550 fluorescence traces of sugar/nutrient responders (top) and fat-only responders (bottom)
551 from 641 neurons of 8 mice, before application of CCKAR blocker (PRE). Stimulus
552 window (10 s for fat or sugar, 60 s for amino acids) is shown by dashed white lines. **b**,
553 POST, to inhibit CCK signalling, we applied devazepide (4 mg/kg, 200 μ L)¹¹, a CCKAR
554 antagonist²⁸ (see Methods for details). Note that blocking CCKAR receptor activation
555 abolishes sugar-, fat- and amino acid-evoked activity in nearly all the nutrient
556 responders (compare POST vs PRE, top panels). By contrast, the CCKAR blocker had
557 no effect on the fat-evoked activity in the fat-only responders (bottom panels). See

558 Extended Data Fig. 6 for results using glutamate receptors blockers. **c**, Cartoon of the
559 gut-to-brain sugar/nutrient sensing vagal axis. The bottom inset illustrates CCK-
560 expressing enteroendocrine cells (EEC) in the intestines. The top inset is a two-
561 dimensional t-distributed stochastic neighbour embedding (tSNE) plot of the
562 transcriptome of mouse vagal nodose neurons³⁷. Shown in red are the clusters
563 expressing CCKAR, and shown in green is the VIP-expressing cluster (see Methods). **d**,
564 Calcium responses in vagal ganglia of animals expressing GCaMP6s in VIP neurons
565 while infusing fat, sugar or amino acids stimuli into the intestines. Heat maps show z-
566 score-normalized fluorescence traces. Approximately 30% of VIP vagal neurons
567 responded to nutrient stimuli ($n=60/203$ neurons from 9 ganglia), but only a very small
568 fraction responded to fat (~4%) responded to fat. Stimuli: 10% linoleic acid, 500mM
569 glucose, 250mM amino acid mixture.

570

571 **Figure 4: VIP vagal neurons convey sugar/nutrient preference**

572 **a**, Silencing VIP neurons in the vagal ganglia by bilateral injection of AAV-DIO-
573 TetTox into the nodose in *Vip-Cre* animals. **b,c**, Fat and sugar preference tests for
574 control mice and mice with silenced VIP-expressing vagal neurons (VIP-Tx). **b**, Control
575 mice develop strong preference for fat during a standard 48 h fat vs. sweetener test
576 ($n=7$). In contrast, silencing of VIP vagal neurons abolishes the development of fat
577 preference ($n=8$, VIP-Tx mice). Two-sided Mann–Whitney U-test, control vs. VIP-Tx fat
578 consumption, $P=3 \times 10^{-4}$. **c**, Silencing of VIP vagal neurons also abolishes the
579 development of sugar preference. Control ($n=7$) versus silenced animals ($n=8$). Two-
580 sided Mann–Whitney U-test, control vs. VIP-Tx sugar consumption, $P = 6 \times 10^{-4}$. Values
581 are mean \pm s.e.m. **d**, Strategy for chemogenetic activation of VIP vagal neurons. An
582 excitatory DREADD receptor (via AAV-DIO-hM3Dq) was targeted bilaterally to the
583 nodose of *Vip-Cre* mice. The mice were then tested for their basal preference to cherry
584 and grape flavour (Pre). Mice were conditioned and tested using the less-preferred
585 flavour plus the DREADD agonist clozapine (Post; see Methods). **e**, Left panel: Control
586 animals (not expressing DREADD) presented with clozapine (5 mg/L) in the less
587 preferred flavour do not switch their preference, and maintain their basal, original flavour
588 choice ($n=8$ mice; two-tailed paired t-test, $P=0.061$). Right panel: After associating

589 clozapine-mediated activation of VIP vagal neurons with the less-preferred flavour, all
590 the animals expressing DREADD switched their preference ($n=6$ mice; two-tailed paired
591 t-test, $P=9.6 \times 10^{-4}$). Preference Index values are mean \pm s.e.m.

592

593 **Figure 5: TRPA1 vagal neurons mediate fat-specific preference**

594 **a**, Single-cell RNA-seq atlas of nodose ganglia³⁷, showing vagal clusters for VIP
595 (blue), *Trpa1* (red), *Gpr65* (orange), *CALCA* (green), *Oxtr* (brown) and *Piezo2* (purple).

596 **b**, The vagal cluster expressing TRPA1 (*Trpa1*-GCaMP6s) responded selectively to
597 intestinal delivery of fat, but not sugar or amino acid stimuli. The heat maps show z-
598 score-normalized fluorescence traces. Of 163 imaged neurons from 5 ganglia, ~24%
599 responded to fat. Stimuli: 10% linoleic acid, 500mM glucose, 250mM amino acid
600 mixture. See Extended Data Fig. 9 for imaging results for the other vagal clusters. **c**,
601 Strategy for silencing of TRPA1 neurons in the vagal ganglia by bilateral injection of
602 AAV-DIO-TetTox into the nodose in *Trpa1*-*Cre* animals. Shown are fat and sugar
603 preference tests for control mice and mice with silenced TRPA1-expressing vagal
604 neurons (*Trpa1*-Tx). Control mice develop strong preference for fat and sugar after 48 h
605 ($n=7$; left panel). In contrast, silencing of TRPA1 vagal neurons abolishes the
606 development of fat but not sugar preference ($n=6$, right panel). Two-sided Mann-
607 Whitney U-test, control vs. *Trpa1*-Tx for sugar, $P=0.23$; control vs. *Trpa1*-Tx for fat, P
608 $=1.1 \times 10^{-3}$. Values are mean \pm s.e.m.

609

610 **Figure 6: Intestinal GPR40 and GPR120 fat receptors activate the gut-brain axis**

611 **a**, We engineered knockout mice for 3 candidate gut fat receptors, and generated
612 all potential knockout combinations. We then recorded vagal responses to intestinal
613 delivery of fat (10% LA) and sugar (500mM glucose), and tested for the development of
614 fat and sugar preference. **b**, Heat maps depict z-score-normalized fluorescence traces
615 from vagal neurons of SGLT1 KO animals in response to intestinal delivery of fat (10%
616 LA) and sugar (500mM glucose). As previously shown, SGLT1 functions as the gut-to-
617 brain sugar receptor⁴, and no vagal neurons responded to sugar in the knockout
618 animals. However, responses to fat are unaffected ($n=174/903$ imaged neurons from 10
619 ganglia). **c**, Heat maps illustrating the selective loss of fat responses in the

620 GPR40/GPR120 double knockout ($n=51/428$ imaged neurons from 6 ganglia) and the
621 triple knockout ($n=44/326$ imaged neurons from 6 ganglia). Note normal responses to
622 intestinal delivery of sugar in these knockout animals. See Extended Data Fig. 10 for
623 imaging results for the other knockout lines. **d**, Bar graphs comparing vagal neurons
624 responding to intestinal delivery of fat (10% LA) in control versus the various receptor
625 knockout combinations (see Methods). Vagal responses were dramatically impacted
626 only in the GPR40/GPR120 double knockout (R40/120, $n=7$, $P=5 \times 10^{-6}$) and in the triple
627 knockout animals (3KO, $n=6$, $P=4 \times 10^{-6}$). Values are mean \pm s.e.m.; Statistics are shown
628 in Methods. **e**, Knockout animals were tested for the development of fat preference.
629 GPR40/GPR120 double knockouts ($n=7$ mice, $P=0.81$) and CD36/GPR40/GPR120
630 triple knockouts ($n=9$ mice, $P=0.46$) do not develop a preference for fat. Open bars:
631 initial preference; red bars: preference at the end of the 48 h test. All other combinations
632 of knockouts are capable of developing behavioural preference for fat, just like control
633 wild-type mice (Statistics are shown in Methods). Values are mean \pm s.e.m. **f**, As
634 expected, GPR40/GPR120 knockouts still develop preference for sugar. Wild type=10
635 mice, $P=2.9 \times 10^{-5}$; R40/120=9 mice, $P=8.0 \times 10^{-5}$; 3KO=7 mice, $P=1.9 \times 10^{-3}$. values are
636 mean \pm s.e.m. (Statistics are shown in Methods).

637

638 **Online Methods**

639

640 **Animals**

641 All procedures were carried out in accordance with the US National Institutes of
642 Health (NIH) guidelines for the care and use of laboratory animals, and were approved
643 by the Institutional Animal Care and Use Committee at Columbia University. Adult
644 animals older than 6 weeks of age and from both genders were used in all experiments.
645 C57BL/6J (JAX 000664), TRAP2 (JAX 030323), *TRPM5* KO (JAX 013068), Ai96 (JAX
646 028866), Ai162 (JAX 031562), *VGlut2-IRES-Cre* (JAX 028863), *Gpr65-IRES-Cre* (JAX
647 029282), *Vip-IRES-Cre* (JAX 010908); *Uts2b-Cre* (JAX 035452); *Piezo2-Cre* (JAX
648 027719); *Oxtr-Cre* (JAX 031303); *Calca-Cre* (JAX 033168); *Snap25-2A-GCaMP6s* (JAX
649 025111), *Penk-IRES2-Cre* (JAX 025112).

650

651 **Generation of genetically modified mice**

652 To engineer *Trpa1-IRES-Cre* knock-in animals⁵¹, an sgRNA (targeting
653 CACAGAACTAAAAGTCCGGG) was selected to introduce an IRES-Cre construct
654 immediately downstream of the endogenous *Trpa1* stop codon. A single-stranded DNA
655 donor containing gene-specific homology arms (150bp each) and the IRES-Cre
656 fragment (Addgene #61574) was generated using the Guide-it Long ssDNA Production
657 System (Takara Bio). Cas9 protein (100 ng/μL), sgRNA (20 ng/μL), and ssDNA donor
658 (10 ng/μL) were co-injected into the pronuclei of fertilised zygotes from B6CBAF1/J
659 parents. Founder pups were screened for the presence of the knock-in allele using
660 PCR, and candidates were validated by Sanger sequencing.

661 SGLT1 knockout mice were generated by co-injecting Cas9 mRNA (100 ng/μl)
662 with sgRNA (50 ng/ul) targeting CGCATTGCGAATGCGCTCGT, resulting in a
663 frameshift after the 20th residue and early termination after the 27th residue (wild type
664 SGLT1 is a 665 aa protein). Homozygous SGLT1 KO mice were bred and maintained
665 on fructose-based rodent diet with no sucrose or cornstarch (Research Diets
666 #D08040105). The mutant allele was validated by DNA sequencing.

667 To generate knockout mice for fat receptors (CD36, GPR40, GPR120), Cas9
668 protein (50 ng/ul) was co-injected with a total of 6 sgRNAs (7 ng/ul each: CD36:
669 AAATATAACTCAGGACCCCG, TAGGATATGGAACCAAAGT; GPR40:
670 AGTGAGTCGCAGTTTACCGT, GAAGTTAGGACTCATCACAG; GPR120:
671 CGACGCTCAACACCAACCGG, ACGCGGAACAAGATGCAGAG). The founder mice
672 were validated by DNA sequencing, and used to generate various homozygous
673 knockout mice (i.e., single, double, triple knockouts). All mutations in the individual
674 homozygous lines were validated by DNA sequencing.

675 To engineer transgenic animals expressing Cre recombinase from the *Cckar*
676 gene (i.e. *Cckar-Cre* animals), a CRE cassette was introduced at the ATG start codon
677 of the CCKAR gene using a 151 Kb BAC (RP23-50P5) carrying the CCKAR gene, as
678 described previously⁵².

679

680

681

682 **Fos stimulation and histology**

683 Stimuli consisted of 20% Intralipid (sc215182, Santa Cruz Biotechnology), 10%
684 linoleic acid, 10% oleic acid, 0.3% xanthan gum, or 10% mineral oil. Stimuli were
685 emulsified by dilution into milliQ water containing 0.1% xanthan gum and 0.05% Tween
686 80, and vortexed for a minimum of 10 min. Note that we used high concentration of IL
687 for cFos and Trap2-labeling experiments to ensure enough IL is consumed and
688 digested during the 90 min stimulation window. In contrast, when performing 48 h
689 behavioral tests examining the development of fat preference, a lower concentration of
690 1.5% IL was used, particularly to ensure that the fat and the AceK (3 mM) are similarly
691 attractive.

692 To motivate drinking behavior during the 90 min cFos induction experiments,
693 C57BL/6J mice were water restricted for 23 h, given access to 1 ml of water for 1 h, and
694 then water restricted again for another 23 h. Previously, we showed that such water
695 restriction prior to the 90 min drinking test did not affect the selectivity of cNST labeling⁴
696 (e.g. no labeling in response to water or AceK; see also Extended Data Fig. 2). Animals
697 had the full complement of food during water restriction (this is essential during Fos
698 labelling experiments as food restriction would activate a wide range of additional
699 circuits, including food-reward circuits upon presentation of sugar or fat stimuli). All Fos
700 experiments consisted of 90 min of exposure to the stimuli; mice were housed
701 individually and all the nesting material and food was removed from their cages. After
702 90 min, mice were perfused transcardially with PBS followed by 4% paraformaldehyde.
703 Brains were dissected and fixed overnight in paraformaldehyde at 4 °C. The brains were
704 sectioned coronally at 100 µm and labelled with anti-c-Fos (SYSY, no. 226004 guinea
705 pig, 1: 5,000) diluted in 1× PBS with 5% normal donkey serum (EMD Millipore, Jackson
706 ImmunoResearch) and 0.3% Triton X-100 for 48 h at 4 °C, and then Alexa Fluor 647-
707 conjugated donkey anti-guinea pig (Jackson ImmunoResearch) for 24 h at 4 °C. Images
708 were acquired using an Olympus FluoView 1000 confocal microscope. Quantification of
709 Fos-labelling was carried out by recording the number of positive neurons in an
710 equivalent 200 x 200 µm area of the cNST (bregma – 7.5 mm) and area postrema.

711 For intragastric stimulation, the catheter was placed as previously described^{4,53}.
712 Mice were individually housed and allowed to recover for at least 5 days before stimulus

713 delivery. A syringe pump microcontroller (Harvard Apparatus) was used to deliver 1.5 ml
714 of the control PBS or 20% IL solution at 0.050 ml/min⁴.

715

716 **Two-bottle preference assays**

717 No behavioral experiments, including the short-term assays for taste responses,
718 or the 48 h tests examining the development of sugar or fat preference used water-
719 restricted or food-deprived animals. Animals were given ad-libitum access to food and
720 water for several days prior to the behavioral tests; any food or water restriction would
721 severely affect the animal's behavior in preference or taste responses.

722 Development of fat preference: Mice were first tested for their initial preference
723 between 1.5% IL and 3 mM AceK ("PRE testing") by completing 100 drinking trials.
724 Each trial was initiated by the first lick and lasted for 5 s; the drinking ports then re-
725 opened after 30 s of inter-trial interval. Next, mice were exposed to 500 licks to both
726 1.5% IL and 3 mM AceK; this was repeated twice. Animals were then tested for the
727 development of fat preference over 36 h using the 5 s trials. The pre- and post-
728 preference indexes were calculated by dividing the number of licks to fat by the total lick
729 count during the first 2-4 h (100 trials) of baseline measurements (PRE) and during the
730 last 2-4 h (100 trials) of the behavioural session (POST), respectively.

731 In order to perform the two-bottle preference assay using large numbers of mice
732 (e.g. Fig. 4b, 5d, and 6e), the setup was modified by using an LCD-based lick counter.
733 The "PRE" preference index was calculated as the number of licks to fat divided by the
734 total lick count during the first 4 hours; the "POST" preference index was calculated as
735 the number of licks to fat divided by the total lick count during the last 4 hours of the
736 session. Mice had ad libitum access to food throughout. The mice with a PRE index >
737 0.75 were not used owing to their high initial preference for fat (less than 20% of total
738 tested mice had to be eliminated due to this strong bias).

739

740 **Fat, sugar and amino acid intestinal stimulation**

741 For nodose imaging experiments: Sugar, 500 mM glucose; amino acids, a mix
742 consisting of 50 mM methionine, 50mM serine, 50 mM alanine, 50 mM glutamine, and
743 50 mM cysteine dissolved in PBS. Fat stimuli: 10% linoleic acid, 10% linolenic acid,

744 10% hexanoic acid, 10% DHA, 10% oleic acid, all diluted in PBS containing 0.1%
745 xanthan gum and 0.05% Tween 80, and vortexed for a minimum of 10 min; vehicle
746 control, 0.1% xanthan gum and 0.05% Tween 80. For sugar and fat intestinal
747 stimulation in imaging experiments, we used a 10s window of stimulation; for amino
748 acids, we used a 60s stimulus, as we used lower concentrations of each in the mix of
749 several amino acids (see above).

750 Note that if using Intralipid mix^{12,13} (a 20% soybean oil emulsion, Santa Cruz) for
751 nodose imaging experiments (rather than consumption where it would be naturally
752 digested and broken down into short, medium and long chain fatty acids), the material
753 needed to be pre-digested with lipases (mimicking its natural course of action upon
754 ingestion). Using the undigested IL for intestinal stimulation imaging experiments
755 yielded unreliable responses (data not shown). IL was incubated with 4mg/ml lipase
756 (sigma) in PBS plus 10 mM CaCl₂ for a minimum of 5 h at 37°C.

758 **Stereotaxic Surgery**

759 Mice were anesthetized with ketamine and xylazine (100 mg/kg and 10 mg/kg,
760 intraperitoneal), and placed into a stereotaxic frame with a closed-loop heating system
761 to maintain body temperature. The coordinates (Paxinos stereotaxic coordinates) used
762 to inject and place recording fibers in the cNST were: caudal 7.5 mm, lateral ±0.3 mm,
763 ventral 3.7–4 mm, all relative to Bregma. The fiber photometry experiments used a 400
764 µm core, 0.48 NA optical fibre (Doric Lenses) implanted 50–100 µm over the left cNST.
765 TRAP2 mice were stereotaxically injected bilaterally in the cNST with AAV9-Syn-DIO-
766 mCherry (300nl/mouse), AAV9 DIO eGFP-RPL10a (300nl/mouse) or AAV9 CBA.FLEX-
767 TetTox (300 nl/mouse)⁵⁴.

769 **Genetic access to fat-preference neurons in the brain**

770 The TRAP strategy was used in TRAP2^{20,55} mice to gain genetic access to fat-
771 activated neurons in the cNST. A minimum of 5 days after injection, the AAV-injected
772 TRAP2 mice or TRAP2; Ai9 mice were water restricted for 23 h, given access to 1 ml of
773 water for 1 h, water restricted again for another 23 h (with ad libitum food), and then
774 presented with 20% Intralipid ad libitum in the absence of food and nesting material.

775 After 1 h, mice were injected intraperitoneally with 12.5 mg/kg 4-hydroxytamoxifen (4-
776 OHT, Sigma H6278) and placed back in the same cage for an additional 3 h. Following
777 4 h of Intralipid exposure, mice were returned to regular home-cage conditions (group-
778 caged, with nesting material, ad libitum food and water). Mice were used for
779 experiments a minimum of 10 days after this TRAP protocol. C57BL/6J and
780 TRAP2 mice expressing TetTox in the cNST were tested in the two-bottle Intralipid
781 versus sweetener preference assay for 48 h, as described previously⁴. Note that
782 animals were not food deprived prior to the 90 min TRAPping, so as to prevent
783 confounds from the activation of feeding and food-reward responding neurons.

784

785 **Fibre photometry**

786 *Vglut2-cre;Ai96* animals were placed in a stereotaxic frame and implanted with a
787 400 μm core, 0.48 NA optical fibre (Doric Lenses) 50–100 μm over the left cNST.
788 Photometry experiments were conducted as described previously^{4,56}. To quantify the
789 effects of vagotomy, we calculated the ratio of stimulus-related peak amplitude of the
790 normalised trace (within 120 s of stimulus onset) prior vagotomy versus after vagotomy.

791 The duodenal catheterization surgery was carried out as described previously⁴.
792 Stimulus delivery was performed via a series of peristaltic pumps (BioChem Fluidics)
793 operated via custom Matlab software/Arduino microcontroller. Stimuli and washes were
794 delivered through separate lines that converged on a common perfusion manifold
795 (Warner Instruments) connected to the duodenal catheter. Trials consisted of a 60-s
796 baseline (PBS 200 $\mu\text{l}/\text{min}$), a 30 s stimulus (200 $\mu\text{l}/\text{min}$), and a 3-min washout period
797 (150 s at 600 $\mu\text{l}/\text{min}$, and 30 s at 150 $\mu\text{l}/\text{min}$). Stimuli were each presented three times
798 in an interleaved fashion. The vagotomy procedure was carried out after the first round
799 of stimulus as described previously^{4,57}.

800

801 **Nodose ganglion injection experiments**

802 Genetic vagal silencing experiments

803 Cre-expressing animals (*Vip-Cre* and *Trpa1-Cre*) were anaesthetized with
804 ketamine and xylazine (100 mg kg⁻¹ and 10 mg kg⁻¹, intraperitoneal). The skin under
805 the neck was shaved and betadine and alcohol were used to scrub the skin three times.

806 A midline incision (~1.5 cm) was made and the trachea and surrounding muscles were
807 gently retracted to expose the nodose ganglia. AAV9 CBA.FLEX-TetTox (600 nl per
808 ganglion) containing Fast Green (Sigma, F7252-5G) was injected in both left and right
809 ganglia using a 30° bevelled glass pipette (custom-bevelled Clunbury Scientific). At the
810 end of surgery, the skin incision was closed using 5-0 absorbable sutures (CP medical,
811 421A). Mice were allowed to recover for a minimum of 26 days before two-bottle
812 preference tests for sugar and fat. We note that almost all of the *Vip-Cre* animals
813 survived the surgical procedure and bilateral injections, while only 50% of the *Trpa1-Cre*
814 animals survived.

815 The *Trpa1-Cre* knock-in line was validated by *in situ* hybridization experiments
816 (Extended Data Fig. 9a). Fixed frozen nodose ganglia were sectioned at 16 µm
817 thickness and processed for mRNA detection using the RNAscope Fluorescent
818 Multiplex Kit (Advanced Cell Diagnostics) following the manufacturer's instructions. The
819 following RNAscope probes were used: *Trpa1* (Cat# 400211-C3) and *Cre-O4* (Cat#
820 546951).

821 Chemogenetic-activation experiments

822 For gain-of-preference experiments, *Vip-Cre* animals were injected bilaterally
823 with 600 nl/ganglion of an AAV carrying the Cre-dependent activator DREADD (AAV9
824 Syn-DIO-hM3Dq-mCherry)^{37,39} and were allowed to recover for a minimum of three
825 weeks before behavioural tests. Control and *Vip-Cre* mice were tested in a two-bottle
826 grape versus cherry flavour-preference assay (grape: 0.39 g/L Kool-Aid Unsweetened
827 Grape, cherry: 0.36 g /L Kool-Aid Unsweetened Cherry, both containing 1 mM AceK).
828 Flavour-preference tests were carried out as previously described⁴.

829

830 **Vagal calcium imaging**

831 Each mouse was anaesthetized with ketamine (100 mg/kg) and xylazine (10
832 mg/kg). The mice were tracheotomized, and the nodose ganglion was exposed for
833 imaging exactly as previously described⁴.

834 For CCKAR blocker experiments, devazepide (sigma) was dissolved in DMSO
835 and diluted to a final dose of 4 mg/kg in saline¹¹. For glutamate receptor blocker
836 experiments, a mixture of metabotropic glutamate receptor antagonist L-(+)-2-Amino-3-

837 phosphonopropionic acid (AP3; 2 mg/kg) and ionotropic glutamate receptor antagonist
838 kynurenic acid (KA, 300 µg/kg) was used. CCKAR and glutamate receptor blockers
839 were delivered both into the intestines and abdominal cavity¹¹; after a 5 min incubation
840 period, the imaging session was started. For CCK application, the intestines, still
841 attached to the anesthetized mouse, were partly placed on a 25mm petri dish to allow
842 delivery (60 s) and wash-out (>180 s) of the stimuli (1 µg/ml CCK peptide; Bachem
843 4033101).

844 Note that for nodose imaging experiments using sugar, glucose stimuli consisted
845 of 10 s pulses since stimulating with high concentration (>250 mM) for long pulses (60 s
846 or more) strongly activates nutrient-independent vagal responses^{4,22,58}, severely
847 masking sugar/nutrient-evoked responses.

848

849 **Calcium-imaging data collection and analysis**

850 Imaging data was obtained using an Evolve 512 EMCCD camera (Photometrics).
851 Data was acquired at 5 Hz. A single field of view was chosen for recording and analysis
852 from each ganglion. Calcium-imaging data collected at 5 Hz was downsampled by a
853 factor of 2, and the images were stabilised using the NoRMCorre algorithm⁵⁹. Motion-
854 corrected movies were then manually segmented in ImageJ using the Cell Magic Wand
855 plugin. Neuropil fluorescence was subtracted from each ROI with the FISSA toolbox⁶⁰,
856 and neural activity was denoised using the OASIS deconvolution algorithm⁶¹.

857 Neuronal activity was analysed for significant stimulus-evoked responses as
858 described previously^{4,62}. Note that for the fat receptor knockout imaging studies, the
859 minimal peak amplitude for defining responders was set to 1% $\Delta F/F$. To quantify
860 responses in fat receptors knockouts (Fig. 6d and Extended Data Fig. 10g), the number
861 of responding neurons over the total number of imaged neurons per ganglia was
862 normalized to the number of responders in wild type control mice (set to 100%).

863 For experiments using blockers, two repeat trials per stimuli were used to
864 accommodate the expanded time scale of the session (i.e. before and after), and a
865 neuron was considered a responder if it responded in both trials. The two-trial average
866 area under curve (AUC) for each stimulus was used to quantify the before and after
867 responses (Extended Data Fig. 6d, e).

868 Imaging data is presented as heat maps of z-score-normalized responses (see
869 also reference 4). Equivalent results are obtained when using absolute $\Delta F/F$ (data not
870 shown)

871

872 **Statistics**

873 No statistical methods were used to predetermine sample size, and investigators
874 were not blinded to group allocation. No method of randomization was used to
875 determine how animals were allocated to experimental groups. Statistical methods used
876 include one-way ANOVA followed by Tukey's HSD post hoc test, two-tailed t-test, two-
877 way ANOVA or the two-sided Mann–Whitney U-test, and are indicated for all figures.
878 Analyses were performed in MATLAB and GraphPad Prism 8. Data are presented as
879 mean \pm s.e.m.

880 Fig. 6d: ANOVA with Tukey's test compared to Snap25-GCaMP6s control. CD36
881 KO (n = 6 mice) vs control, $P = 0.99$; GPR40 KO (R40, n = 7 mice) vs control, $P = 0.89$;
882 GPR120 KO (R120, n = 6 mice) vs control, $P = 0.53$; CD36/GPR40 double KO
883 (CD36/R40, n = 6 mice) vs control, $P = 0.96$; CD36/GPR120 double KO, (CD36/R120, n
884 = 8 mice) vs control, $P = 0.99$; GPR40/GPR120 double KO (R40/120, n = 7 mice) vs
885 control, $P = 5 \times 10^{-6}$; CD36/GPR40/GPR120 triple KO (3KO, n = 6 mice) vs control, $P =$
886 4×10^{-6} .

887 Fig. 6e: Two-tailed paired t-tests evaluating Pre versus Post fat preference. Wild
888 type mice (WT, n = 11 mice) Pre vs Post, $P = 2 \times 10^{-6}$; CD36 KO, (n = 8 mice) Pre vs
889 Post, $P = 4.8 \times 10^{-3}$; GPR40 KO, (R40, n = 12 mice) Pre vs Post, $P = 1 \times 10^{-4}$; GPR120
890 KO, (R120, n = 14 mice) Pre vs Post, $P = 1.03 \times 10^{-4}$; CD36/GPR40 KO, (D36/R40, n = 5
891 mice) Pre vs Post, $P = 2 \times 10^{-2}$; CD36/GPR120 KO (D36/R120, n = 6 mice) Pre vs Post,
892 $P = 1.7 \times 10^{-3}$; GPR40/GPR120 double KO (R40/120, n = 7 mice) Pre vs Post, $P = 0.81$;
893 CD36/GPR40/GPR120 triple KO (3KO, n = 9 mice) Pre vs Post, $P = 0.46$.

894 Fig. 6f: Two-tailed paired t-tests evaluating Pre versus Post sugar preference.
895 Wild type mice (WT, n = 10 mice) Pre vs Post, $P = 2.9 \times 10^{-5}$; GPR40^{-/-}GPR120^{-/-}
896 (R40/120, n = 9 mice), Pre vs Post, $P = 8.0 \times 10^{-5}$; CD36^{-/-}GPR40^{-/-}GPR120^{-/-} (3KO, n = 7
897 mice), Pre vs Post, $P = 1.9 \times 10^{-3}$.

898

899 **Code availability**

900 Custom code is available from corresponding author upon request.

901

902 **Data availability**

903 All data supporting the findings of this study are available upon request.

904

905 **References for Methods and Supplementary Information**

- 906 51. Yang, H., Wang, H. & Jaenisch, R. Generating genetically modified mice using
907 CRISPR/Cas-mediated genome engineering. *Nat Protoc* **9**, 1956-1968, (2014).
- 908 52. Lee, H., Macpherson, L. J., Parada, C. A., Zuker, C. S. & Ryba, N. J. P. Rewiring
909 the taste system. *Nature* **548**, 330-333, (2017).
- 910 53. Ueno, A. *et al.* Mouse intragastric infusion (iG) model. *Nat Protoc* **7**, 771-781,
911 (2012).
- 912 54. Murray, A. J. *et al.* Parvalbumin-positive CA1 interneurons are required for
913 spatial working but not for reference memory. *Nat Neurosci* **14**, 297-299, (2011).
- 914 55. DeNardo, L. A. *et al.* Temporal evolution of cortical ensembles promoting remote
915 memory retrieval. *Nat Neurosci* **22**, 460-469, (2019).
- 916 56. Lerner, T. N. *et al.* Intact-Brain Analyses Reveal Distinct Information Carried by
917 SNc Dopamine Subcircuits. *Cell* **162**, 635-647, (2015).
- 918 57. Allen, I. C. Mouse Models of Allergic Disease Methods and Protocols Preface.
919 *Mouse Models of Allergic Disease, Methods and Protocols* **1032**, V-Vi, (2013).
- 920 58. Ichiki, T. *et al.* Sensory representation and detection mechanisms of gut
921 osmolality change. *Nature* **602**, 468-474, (2022).
- 922 59. Pnevmatikakis, E. A. & Giovannucci, A. NoRMCorre: An online algorithm for
923 piecewise rigid motion correction of calcium imaging data. *J Neurosci Methods*
924 **291**, 83-94, (2017).
- 925 60. Keemink, S. W. *et al.* FISSA: A neuropil decontamination toolbox for calcium
926 imaging signals. *Sci Rep* **8**, 3493, (2018).
- 927 61. Friedrich, J., Zhou, P. & Paninski, L. Fast online deconvolution of calcium
928 imaging data. *PLoS Comput Biol* **13**, e1005423, (2017).

- 929 62. Barretto, R. P. *et al.* The neural representation of taste quality at the periphery.
930 *Nature* **517**, 373-376, (2015).
- 931 63. Madisen, L. *et al.* A robust and high-throughput Cre reporting and
932 characterization system for the whole mouse brain. *Nat Neurosci* **13**, 133-140,
933 (2010).

934

935 **Acknowledgements**

936 We thank members of the Zuker lab for valuable comments and suggestions,
937 and an extraordinary group of undergraduate students from Columbia University that
938 participated in various aspects of this work, Andre Balian, Justine Li, and Brian McTyre.
939 We particularly thank Liqun Luo (Stanford University) for the generous gift of TRAP
940 animals, Alex Sisti for the generation of SGLT1 knockout mice, Hao Jin for general
941 advice with figures and experiments, Zaiqi (Julie) Wu for help generating the genetically
942 engineered animals, and Laura Rickman for expert help with figures. H-E.T. was
943 supported by Agency for Science, Technology and Research and National Medical
944 Research Council of Singapore. Research reported in this publication was supported in
945 part by the Russell Berrie Foundation program in the neurobiology of obesity (to C.S.Z
946 and Rudy Leibel). C.S.Z. is an investigator of the Howard Hughes Medical Institute.
947 Figures were generated with the help of BioRender.

948 This article is subject to HHMI's Open Access to Publications policy. HHMI lab
949 heads have previously granted a nonexclusive CC BY 4.0 license to the public and a
950 sublicensable license to HHMI in their research articles. Pursuant to those licenses, the
951 author-accepted manuscript of this article can be made freely available under a CC BY
952 4.0 license immediately upon publication.

953

954 **Author Contributions**

955 M.L. designed the study, carried out the experiments, developed the imaging
956 strategies, and analysed data. H-E.T. carried out the initial studies, engineered animals
957 and generated fat receptor knockout animals. Z.L. helped with generating knock-in
958 lines, molecular studies, single cell RNA seq analysis, and analysed data. K.S.T.
959 designed and characterized engineered animals and behavioural experiments, and

960 analysed data. A.J.C. performed physiological and behavioural experiments. C.S.Z.
961 designed the study and analysed data. C.S.Z. and M.L. wrote the paper with input from
962 other authors. H-E.T. current address: Agency for Science, Technology and Research,
963 Singapore 138668, Singapore.

964

965

966 **Competing Interests**

967 C.S.Z. is a scientific co-founder and advisor of Kallyope

968

969 **Extended Data Figure legends**

970

971 **Extended Data Figure 1: Development of post-ingestive fat preference is** 972 **independent of immediate attraction to fat and caloric content**

973 **a,b**, Immediate attraction to sweet and fat. Graphs of lick counts from brief-
974 access (30 min) two-bottle tests. **a**, Artificial sweetener (3 mM AceK) versus water, $n = 9$
975 mice, two-tailed paired t-test, $P = 2 \times 10^{-6}$; **b**, Fat (1.5% Intralipid, IL) versus water, $n = 9$
976 mice, two-tailed paired t-test, $P = 2 \times 10^{-5}$. Values are mean \pm s.e.m. Note strong innate
977 attraction to sweet and fat stimuli. **c**, Immediate attraction to fat is abolished in TRPM5
978 knock-out animals. Shown are results from 30 min two-bottle test of fat (1.5% Intralipid,
979 IL) versus water in wild type mice (left panel, $n = 11$ mice) versus TRPM5 knockout
980 mice (right panel, $n = 12$ mice). TRPM5 knock-out animals are blind to the taste of fat³.
981 Two-sided Mann–Whitney U-test wild type versus TRPM5 knockout fat consumption: P
982 = 1.6×10^{-3} . Note that there is no innate attraction to either bottle, with the animals
983 randomly choosing to consume from either one. **d**, In contrast, in a 48 h two-bottle fat
984 preference test, TRPM5 KO animals still developed strong post-ingestive preference to
985 fat ($n = 6$ mice, two-tailed paired t-test, $P = 7.4 \times 10^{-4}$). **e**, Development of fat preference
986 is independent of caloric content. To test the effect of calories, we examined preference
987 between a caloric sugar (fructose) versus fat. Importantly, we used a sugar (fructose)
988 that does not activate SGLT1, and therefore does not trigger post-ingestive preference⁴,
989 thus we can isolate the effect of calories without the confound of having two preference-
990 triggering stimuli (i.e. glucose versus fat). Cartoon on the top illustrates the behavioral

991 arena; mice were allowed to choose between fructose (0.15 kcal/ml) and fat (IL at 0.15
992 kcal/ml). **f**, Similar test, but fructose at twice (0.3 kcal/ml) the caloric content of IL. By
993 the end of the 48 h preference test, all the mice switched their preference for fat. **e**,
994 paired t-test, $P = 8 \times 10^{-4}$, $n = 7$; **f**, paired t-test, $P = 1 \times 10^{-5}$, $n = 7$. Note that while at the
995 higher fructose concentration (panel **f**) all of the animals began the test with much
996 stronger attraction to the (sweeter) fructose bottle, all still switched their preference to
997 fat, independent of caloric content.

998

999 **Extended Data Figure 2: Fat activates cNST neurons**

1000 **a-d**, Strong Fos labelling is observed in neurons of the cNST (Bregma -7.5mm) in
1001 response to ingestion of fat stimuli (panels **c-d**), but not in control animals (10% mineral
1002 oil, panel **b**). Stimulus: 10% linoleic acid (LA), 10% oleic acid (OA). Scale bars, 200 μm .
1003 **e**, Quantification of Fos-positive neurons. ANOVA with Tukey's HSD test against
1004 mineral oil (MO, $n = 5$ mice): $P = 3.4 \times 10^{-5}$ for linoleic acid (LA, $n = 5$ mice), $P = 3.9 \times 10^{-5}$
1005 for oleic acid (OA, $n = 5$ mice). Values are mean \pm s.e.m. **f-i**, TetTox silencing of fat-
1006 TRAP cNST neurons does not impair immediate attraction to sweet (3 mM AceK; **f, g**)
1007 or fat (1.5% IL; **h, i**). Two-tailed paired t-tests: sweet versus water, wild type, $n = 10$, $P =$
1008 1.1×10^{-7} ; TetTox $n = 9$, $P = 1.1 \times 10^{-6}$. For fat versus water, wild type, $n = 10$, $P = 6.8 \times 10^{-$
1009 5 ; TetTox, $n = 9$, $P = 1.7 \times 10^{-5}$. Values are mean \pm s.e.m. **j-k**, Intragastric infusion with fat
1010 activates cNST neurons. **j**, Direct intragastric infusion of fat (IL) but not control (PBS)
1011 robustly activates the cNST. Scale bars, 100 μm . **k**, Quantification of Fos-positive
1012 neurons in animals infused with control and IL stimuli, Two-sided Mann-Whitney U-test
1013 between control and Intralipid ($n = 5$ mice), $P = 8 \times 10^{-3}$. **l**, We note that we often observe
1014 variable labeling in the area postrema (see Figure 1c and panel j here), but such
1015 labeling is independent of oral versus intragastric infusion⁴. The bar graphs show the
1016 quantification of Fos⁺ neurons in the area postrema (AP) and cNST (Fig. 1d) in
1017 response to free licking of IL (90 min) versus intragastric infusion ($n = 5$ mice). cFos in
1018 cNST: oral 105 ± 6 , infusion 99 ± 6 , cFos in AP: oral 93 ± 15 , infusion 90 ± 12 . The
1019 equivalent area of the cNST (bregma - 7.5 mm) was processed and counted for the
1020 different experiments. Two tailed unpaired t-test, cNST: $P = 0.54$; AP: $P = 0.86$. Values
1021 are mean \pm s.e.m.

1022 **Extended Data Figure 3: Quantification of cNST and nodose labeling**

1023 **a**, Genetic TRAPing of cNST neurons with fat stimuli (see Methods) is efficient
1024 and reliable. We labelled the fat-induced TRAP2 neurons by infection with an AAV
1025 carrying a Cre-dependent fluorescent reporter⁴ (shown in green), and then performed a
1026 second cycle of fat stimulation followed by Fos antibody labelling⁴ (shown in red; see
1027 Methods). **b**, By comparing the number of neurons expressing the fluorescent reporter
1028 to the number neurons labelled by Fos antibodies, we determined that $90.7 \pm 0.6\%$ of
1029 Fat-Fos neurons were also TRAPed with the fat stimuli ($n = 6$). Scale bar, 20 μm . **c**, For
1030 experiments targeting AAV- FLEX-TetTox, or AAV-DIO-mCherry (or GFP) to the cNST
1031 we used fat-stimulated TRAP2 animals (see Methods). By comparing the number of
1032 neurons expressing AAV after TRAPing and infection, to the number of cNST neurons
1033 labeled after crossing similarly TRAPed animals to Ai9⁶³ reporter mice, we estimate the
1034 infection of TRAPed neurons to be $>90\%$: TRAP-AAV: 68 ± 1 neurons; Trap-Ai9: 71 ± 1
1035 neurons ($n = 8$). Scale bar, 100 μm . The equivalent area of the cNST (bregma $- 7.5$
1036 mm) was processed and counted for the separate experiments. Values are mean \pm
1037 s.e.m. **d**, Shown is a whole mount image of a nodose ganglia from *Vip-Cre* animals
1038 infected with AAV- FLEX-TetTox virus (see Methods). Average number of labeled
1039 neurons from *Vip-TetTox* was 48 ± 13 neurons ($n = 4$), and the average of nodose
1040 neurons labeled with AAV- FLEX-TetTox virus in the *Trpa1-Cre* animals was 62 ± 23
1041 neurons ($n=6$; not shown). These numbers compare favorably ($\sim 50\%$) to the total
1042 number of VIP and *Trpa1* neurons detected by crossing the Cre animals to reporter
1043 Ai9⁶³ mice: VIP ~ 100 neurons; *Trpa1* ~ 120 neurons (data not shown). Scale bar, 100
1044 μm . **e**, Shown is a whole mount image of nodose ganglia from *Vip-Cre* animals infected
1045 with AAV- DIO-hM3Dq (activator DREADD^{36,38}). VIP-DREADD labeling efficiency:
1046 $43 \pm 4\%$ ($43 \pm 4 / 100.5$), $n = 9$. Scale bar, 100 μm . **f-i**, cNST-activation in response to
1047 intestinal delivery of fat and sugar is mediated via vagal signaling. AAV carrying a Cre-
1048 dependent GCaMP6s was targeted to the cNST of *Penk-Cre* animals⁴. **f**, Fiber
1049 photometry was used to monitor cNST activity in response to intestinal delivery of sugar
1050 and fat stimuli (see also Fig. 2b-d); to minimize any labeling in the AP and ensure the
1051 signals originate in cNST neurons, we used AAV targeting of GCaMP6s to the cNST
1052 (see panel I below). **g**, Neural responses following intestinal delivery of fat (10% linoleic

1053 acid, LA) or sugar (500 mM glucose, Glu). The light traces denote normalized three-trial
1054 averages from individual animals, and the dark trace is the average of all trials. The
1055 responses after bilateral vagotomy are shown in green. Black bars below traces indicate
1056 the time and duration of stimuli; $n = 4$ mice. NR, normalized response. Note robust,
1057 time-locked responses of cNST neurons to intestinal delivery of fat and sugar.
1058 Importantly, responses are abolished after bilateral vagotomy. **h**, Quantification of
1059 neural responses before and after vagotomy. Two-tailed paired t-test, $P = 3.8 \times 10^{-5}$
1060 (sugar), $P = 5 \times 10^{-5}$ (fat). Data are mean \pm s.e.m. **i**, Sample brains of two different
1061 injected animals demonstrating expression of GCaMP6s restricted to the cNST, with
1062 minimal expression in the AP; the top brain also demarks the location of the recording
1063 fiber (dashed rectangle). Scale bars, 200 μ m.

1064

1065 **Extended Data Figure 4: Various dietary fatty acids activate vagal neurons**

1066 **a-b**, Schematic of vagal calcium imaging while simultaneously delivering stimuli
1067 into the intestines (see Methods for details). The picture shows a representative view of
1068 a vagal nodose ganglion of *Vglut-Cre; Ai96* in an imaging session. Two fat responders
1069 (denoted #1 and #2) are highlighted, and their responses shown in panel c. **c**, Sample
1070 traces of vagal responses to intestinal stimulation with alternating pulses of vehicle or
1071 fat (pre-digested IL; see Methods for details). Note time-locked, reliable responses to
1072 fat, but not to vehicle control. Stimulus window (60 s) is marked by dotted white lines.
1073 Note that since IL is a complex mix, it must be pre-digested in vitro by incubation with
1074 lipases prior to using in imaging experiments (versus ingestion, where endogenous
1075 lipases in the stomach naturally digest IL). **d**, Heat maps depict z-score-normalized
1076 fluorescence traces from vagal neurons that responded to pre-digested (dIL, $n = 79/463$
1077 neurons from 8 ganglia). Each row represents the average activity of a single cell to
1078 three trials. Stimulus window is shown by dotted white lines. **e-i**, Responses of vagal
1079 neurons to intestinal delivery of a range of fatty acids. **e**, Heat maps show z-score-
1080 normalized fluorescence traces of vagal neurons to intestinal delivery of 10% LA (10 s)
1081 and digested Intralipid (dIL); $n = 116/634$ neurons from 7 ganglia; note that the same
1082 neurons responded to both stimuli. **f**, 10% LA (10 s) and 10% alpha-linolenic acid (ALA),
1083 $n = 49/322$ neurons from 3 ganglia; **g**, 10% LA (10 s) and 10% docosahexaenoic acid

1084 (DHA), $n = 51/348$ neurons from 5 ganglia; **h**, 10% LA (10 s) and 10% oleic acid (OA),
1085 $n = 39/418$ neurons from 6 ganglia; **i**, 10% LA (10 s) and 10% hexanoic acid (HA),
1086 $n = 52/495$ neurons from 6 ganglia.

1087

1088 **Extended Data Figure 5: Distinct populations of vagal neurons respond to**
1089 **intestinal delivery of nutrients and fat**

1090 **a**, Pie chart illustrating the fraction of fat and sugar responders in the nodose
1091 ganglia of Vglut2-GCaMP6s animals. The data is from 1813 neurons from 22 ganglia
1092 (red, $n = 323$ cells, 17%). Right, within the responding neurons, 151 (47%) responded to
1093 both sugar and fat (“nutrient responders”), while 153 (47%) responded only to fat but not
1094 to sugar stimuli (“fat-only responders”). **b**, Sugar/nutrient versus fat-only vagal neurons:
1095 Heat maps depicting z-score-normalized vagal responses to intestinal delivery of fat
1096 (10% linoleic acid, LA), sugar (500 mM glucose) and amino acids (250 mM amino acid
1097 mixture, AA; see Methods). Each row represents the average activity of a single cell to 3
1098 trials. Stimulus window is shown by dotted white lines. Upper panels show 150 neurons
1099 that responded to intestinal application of sugar, fat and amino acids (“sugar/nutrient
1100 responders”); bottom panels show 192 neurons that responded only to fat. $n = 22$
1101 ganglia, 1884 imaged neurons. **c**, Representative traces from a “sugar/nutrient
1102 responder” (top) and a “fat-only responder” (bottom). Shown are responses to intestinal
1103 stimulation with 9 interleaved pulses of fat (10% LA, 10 s, green dotted line), sugar (500
1104 mM Glu, 10 s) and amino acids (250 mM AA, 60 s). **d**, Heat maps of the small subset of
1105 vagal neurons that responded to sugar and amino acids but not to fat ($n = 14/1884$
1106 neurons from 22 nodose ganglia). On average, less than 1 neuron was detected per
1107 ganglia. We note that when using high concentrations of glucose stimuli (>250 mM) for
1108 long stimulation times (60 s) one can detect strong vagal responses, but these have
1109 been shown not to be sugar-preference responses^{4,22}.

1110

1111 **Extended Data Figure 6: CCK signalling mediates sugar/nutrient responses**

1112 **a**, Cartoon of vagal calcium imaging while simultaneously delivering sugar and fat
1113 stimuli into the intestines. The bottom inset illustrates CCK-expressing enteroendocrine
1114 cells (EECs) in the intestines. **b**, A recent study¹¹ reported that the gut-to-vagal sugar

1115 preference signal is carried by glutamate as a transmitter²⁶. However, this conclusion
1116 was based on three indirect assays and measurements. First, the use of in vitro
1117 organoids with dissociated vagal neurons, where all native connectivity between
1118 potential EECs and vagal neurons is lost²⁶. Second, by using whole nerve recordings
1119 from thousands of random vagal fibres¹¹, which do not afford the identification of the
1120 functionally relevant vagal signal (i.e. recognizing the sugar-preference signals from any
1121 other activity). Third, by using very long sugar stimuli (1 min) under conditions known to
1122 activate large populations of vagal neurons that mask the response of sugar/nutrient
1123 preference neurons^{4,22,58} (note also that the whole vagal nerve responses, unlike
1124 sugar/nutrient responses, never decayed after termination of the sugar stimulus).
1125 Consequently, we directly examined the role of glutamate signalling by imaging the
1126 responses of the relevant sugar-preference vagal neurons to intestinal sugar stimuli
1127 before and after addition of a mixture of AP3 and KA glutamate receptor
1128 antagonists. Indeed, our results demonstrated that pharmacological inhibition of
1129 glutamate-based signalling has no effect on this gut-to-vagal sugar/nutrient sensing
1130 circuit. Shown are representative traces of vagal neuron responses to intestinal
1131 infusions of fat, sugar and amino acids before and after treatment with
1132 ionotropic/metabotropic glutamate receptor antagonists (2 mg/kg AP3 with 300 µg/kg
1133 kynurenic acid, see Methods). Top traces show sugar/fat/amino acid responding vagal
1134 neurons, bottom traces show fat-only responders. **c**, In contrast, pharmacological
1135 inhibition of glutamate-based signalling abolished all osmolarity responses. Heat maps
1136 depicting z-score-normalized vagal responses to intestinal osmolarity stimuli (60s of 1 M
1137 NaCl)^{4,22,58} before and after treatment with ionotropic/metabotropic glutamate receptor
1138 antagonists (2 mg/kg AP3 with 300 µg/kg kynurenic acid). **d**, Quantification of the
1139 responses to 1 M NaCl, 10% LA, 500 mM Glucose, and 250 mM AA mixture before
1140 (black bars) and after blockers (red bars). 1M NaCl, $n = 56$ neurons, $P = 1 \times 10^{-10}$. For
1141 nutrient responders: LA, $n = 21$, $P = 0.16$; Glucose, $n = 21$, $P = 0.85$; AA, $n = 21$, $P =$
1142 0.07 . For fat-only responders, $n = 19$, $P = 0.54$ by two-tailed paired t-tests. All values
1143 are mean \pm s.e.m. AUC: average area under curve (see Methods). **e**, Left,
1144 Representative traces of vagal neuron responses to intestinal infusions of fat, sugar and
1145 amino acids before and after treatment with cholecystinin A receptor (CCKAR)

1146 blocker (4 mg/kg devazepide, see Methods). Note robust, reliable responses to fat (10%
1147 LA) and sugar (500 mM Glucose) prior to addition of CCKAR antagonist. However, all
1148 responses are lost after addition of antagonist (top panel). By contrast, fat-only
1149 responses are unaffected (bottom panel). Right panel, quantification of responses
1150 before (open bars) and after (red bars) CCKAR antagonist (data from Fig. 3a, b). For
1151 nutrient responders: LA, $n = 37$ neurons, $P = 1 \times 10^{-9}$; Glucose, $n = 37$, $P = 1 \times 10^{-9}$; AA, n
1152 $= 37$, $P = 1 \times 10^{-9}$. For fat-only responders, $n = 38$, $P = 0.11$ by two-tailed paired t-tests.
1153 All values are mean \pm s.e.m. **f**, Sugar/nutrient but not fat-only responders utilise CCK
1154 signalling. Left, Heat maps depicting z-score-normalized fluorescence traces from vagal
1155 neurons identified as sugar/nutrient responders (upper panels, $n = 41$ neurons); note
1156 responses to sugar, fat and amino acid stimuli. The lower heat-map shows the fat-only
1157 neurons ($n = 41$ neurons). After stimulating with CCK (1 μ g/ml), all sugar/nutrient
1158 responders were activated, but not the fat-only vagal neurons. Right, Representative
1159 traces of 2 sample neurons to pulses of 10% linoleic acid (LA), 500 mM glucose (G),
1160 250 mM amino acids (A), and CCK. Stimulus windows are indicated by dotted lines. **g-**
1161 **h**, CCK-dependent (sugar and fat) and CCK-independent (fat-only) intestinal gut-to-
1162 brain fat-preference pathways co-contribute to fat signals in the cNST. Shown are
1163 photometric recordings of cNST neurons in *Penk-Cre* animals⁴ in response to intestinal
1164 fat-evoked activation of both fat-stimulated vagal pathways (black traces and bars).
1165 Shown in red are the same responses after inhibiting signaling via the CCK-dependent
1166 vagal pathway (see panel a-f). **i**, cNST responses to intestinal fat stimulation are
1167 reduced to ~50% after removing CCK-dependent signaling, demonstrating the separate
1168 contributions of the two fat-preference circuits. As expected, sugar-evoked responses
1169 are completely abolished after inhibiting signaling via the CCK-dependent pathway. $n =$
1170 5 , $P = 2.4 \times 10^{-6}$ by two-tailed paired t-test. All values are mean \pm s.e.m. See text and
1171 methods for details. We note that in gain-of-function experiments, with DREADD being
1172 overexpressed in vagal neurons, activation of a single pathway is sufficient to create
1173 new preferences (see for example Fig.4).

1174
1175
1176

1177 **Extended Data Figure 7: Sugar/fat/amino acid sensing vagal neurons**

1178 **a**, Shown is a tSNE plot of the transcriptome of mouse vagal nodose neurons
1179 (original data set taken from reference³⁷); CCKAR expression is represented on a grey-
1180 to-red scale. **b**, CCKAR-expressing neurons respond to intestinal stimulation with
1181 nutrients. An engineered *Cckar-iCre* was used to drive GCaMP6s expression in CCKAR
1182 vagal neurons (see Methods). We analysed 724 imaged neurons from 12 ganglia.
1183 Shown are heat maps depicting z-score-normalized fluorescence traces of the CCKAR-
1184 expressing neurons responding to intestinal delivery of fat (10 % linoleic acid), sugar
1185 (500 mM glucose) or amino acids (250 mM amino acid mixture). Stimulus window is
1186 shown by dotted white lines. **c-d**, tSNE plot of the transcriptome of mouse vagal nodose
1187 neurons; urotensin 2B (*Uts2b*) expression is represented on a grey-to-red scale. **d**,
1188 Shown are responses of vagal *Uts2b*-expressing neurons (*Uts2b*-GCaMP6s) to
1189 intestinal delivery of fat (10 % linoleic acid), sugar (500 mM glucose) or amino acids
1190 (250 mM amino acid mixture). The heat maps depict z-score-normalised fluorescence
1191 traces of sugar/nutrient responders ($n = 52/207$ neurons from 7 ganglia). Stimulus
1192 window is shown by dotted white lines. Note that only 3 of the 52 neurons responded
1193 only to fat (shown at the top of the heat maps). **e**, Sugar/nutrient responders are a
1194 unique subset of CCKAR-expressing vagal neurons. Heat maps showing z-score-
1195 normalized fluorescence traces from vagal neurons that respond to CCK and nutrient
1196 stimuli (see Extended Data Fig. 6f). While all of the neurons that responded to intestinal
1197 stimulation with sugar, fat and amino acids (i.e. the sugar/nutrient sensors) also
1198 responded to CCK, the vast majority of vagal neurons that respond to CCK do not
1199 respond to nutrient stimuli (bottom heat maps, $n = 136$ neurons). This is expected since
1200 only a small fraction would be mediating sugar/nutrient preference, versus other roles of
1201 CCK signaling³¹⁻³³. Stimuli: 10% linoleic acid (LA), 10 s; 500 mM glucose, 10 s; 250 mM
1202 amino acids (AA), 60 s; 1 $\mu\text{g/ml}$ CCK, 60 s. **f**, the pie chart is based on data from 12
1203 ganglia. Since vagal neurons that only respond to fat stimuli are not activated by CCK,
1204 they are not part of this analysis (see Extended Data Fig. 6f, bottom panels). **g**, Pie
1205 charts depicting the fraction of sugar/nutrient (red) and fat-only (green) responders in
1206 animals driving GCaMP6s reporter from various driver lines: *Vglut2-Cre*, *Cckar-Cre*,

1207 *Vip-Cre*, *Uts2b-Cre*, and *Trpa1-Cre* animals. *VIP/Uts2b* define the sugar/nutrient
1208 responders while *TrpA1* mark the fat-only responders.

1209

1210 **Extended Data Figure 8: Drinking and eating in Tet-Tox silenced animals.**

1211 **a**, Shown are graphs for consumption (AceK and IL) in two-bottle 48 h preference
1212 assay for control and cNST-silenced animals ($n \geq 8$ mice), $P = 0.151$ (from Fig.2a). **b**,
1213 Consumption in two-bottle 48 h preference assay for control and *Vip*-silenced mice ($n \geq$
1214 7 mice), $P = 0.69$ (from Fig. 4b). **c**, Consumption in two-bottle 48 hr preference assay
1215 for control and *Trpa1*-silenced mice ($n \geq 6$ mice), $P = 0.44$ (from Fig. 5c). Values are
1216 mean \pm s.e.m. **d-f**, Animals with genetically silenced sugar/nutrient preference vagal
1217 neurons (*VIP*), or fat-only vagal neurons (*Trpa1*) still exhibit normal innate attraction to
1218 sweetener (**d**), sugar (**e**), and fat stimuli (**f**). Shown are graphs for 30 min two-bottle
1219 tests for control mice, and for mice with silenced *VIP*-expressing vagal neurons (*VIP-Tx*)
1220 and mice with silenced *Trpa1*-expressing vagal neurons (*Trpa1-Tx*). **d**, AceK versus
1221 water in *VIP-Tx* ($n = 8$) and *Trpa1-Tx* ($n = 6$) animals is not significantly different from
1222 controls. ANOVA with Tukey's test: *VIP-Tx*, $P = 0.36$, *Trpa1-Tx*, $P = 0.66$. **e**, Glucose
1223 versus water in *VIP-Tx* ($n = 8$) and *Trpa1-Tx* ($n = 6$) is not significantly different from
1224 control animals. ANOVA with Tukey's test: *VIP-Tx*, $P = 0.45$, *Trpa1-Tx*, $P = 0.67$. **f**, IL
1225 versus water in *VIP-Tx* ($n = 8$) and *Trpa1-Tx* ($n = 6$) is not significantly different from
1226 control animals. ANOVA with Tukey's test: *VIP-Tx*, $P = 0.87$, *Trpa1-Tx*, $P = 0.91$. Values
1227 are mean \pm s.e.m. Tastants: AceK (3 mM), Glucose (200 mM), IL (1.5%). **g**, The graph
1228 shows body weight measurements from *Vip-Cre* animals injected with AAV-Flex-TetTox
1229 in both nodose ganglia, from the time the animals were infected until the time behavioral
1230 preference tests were performed (days 24- 26.); data is presented as percent change,
1231 with weight at time zero defined as 100%. Thin lines represent individual animals; dark
1232 lines represent the average body weight of TetTox ($n = 7$ mice, red) and control ($n = 10$
1233 mice, black) animals. No significant differences were detected, two-way ANOVA, $P =$
1234 0.37.

1235

1236

1237

1238 **Extended Data Figure 9: Gpr65, Piezo2, Calca, and Oxtr vagal neurons do not**
1239 **sense fat or sugar**

1240 **a**, Validation of *Trpa1-Cre* mice. Double *In situ* hybridization labeling for the
1241 endogenous *Trpa1* gene (green) and for Cre-recombinase (red) in the nodose of *Trpa1-*
1242 *Cre* knock-in mice (see Methods). Shown is a frozen section demonstrating the strong
1243 overlap ($n = 3$ mice). The left 3 panels show the in-situ results, and the right 3 panels
1244 show an illustration of the labeling results. Scale bars, 100 μm . **b-e**, The panels show
1245 tSNE plots of the nodose transcriptome³⁷ highlighting the 4 clusters, and heat maps of
1246 responses to intestinal delivery of fat and sugar from various vagal clusters using the
1247 corresponding Cre driver lines. **a**, GPR65 vagal neurons are known to indiscriminately
1248 respond to a wide range of long stimuli at high concentrations, including salt, fructose,
1249 mannose, and glucose, and considered osmolarity responders^{4,22,58}. The heat maps
1250 show z-score-normalized fluorescence traces from all imaged vagal neurons in
1251 response to intestinal infusions of fat (10% linoleic acid, LA, 10 s), sugar (500 mM
1252 glucose, 10 s) or high osmolarity salt (1 M NaCl) for 60s in *Gpr65-Cre;Ai96* animals.
1253 Each row represents the average activity of a single cell to three trials. Stimulus window
1254 is shown by dotted white lines. $n = 69$ neurons from 3 ganglia. **c-e**, Calcium imaging of
1255 vagal responses in *Piezo2-Cre;Ai96*, *Calca-Cre;Ai96*, and *Oxtr-Cre;Ai96* animals. The
1256 heat maps showing z-score-normalized fluorescence traces of all imaged neurons in
1257 response to intestinal infusion of fat or sugar. **c**, Piezo2: $n = 99$ neurons from 4 ganglia;
1258 **d**, Calca: $n = 168$ neurons from 5 ganglia; **e**, Oxtr: $n = 89$ neurons from 6 ganglia. No
1259 significant responses were detected for any of the lines. **f**, Generation of fat receptor
1260 knockouts. Schematic illustrating the structural domains of the murine wild type CD36,
1261 GPR40, and GPR120 protein sequences, with the deletions denoted by the black
1262 boxes. For CD36 KO, we engineered a 626 nucleotide (nt) deletion removing residues
1263 107 to 185, which forms part of the hydrophobic binding pocket of CD36⁴⁴. For GPR40
1264 KO, we engineered a 695 nt deletion that removed more than 75% of the protein. For
1265 GPR120, we introduced a 412 nt deletion removing 136 residues, and introducing a
1266 nonsense frameshift disrupting functional translation of the remaining two-thirds of the
1267 protein. See Methods for details. **g**, Representative views of GCaMP6s expressing
1268 neurons in vagal nodose imaging sessions using *Vglut2-Cre; Ai96* animals (left) or

1269 Snap25-GCaMP6s animals (right). Scale bar, 100 μ m. Similar results were obtained
1270 from multiple animals. **h**, Comparisons of the fraction of sugar/nutrient responders (left)
1271 or fat-only responders (right), between *Vglut2-Cre; Ai96* (*Vglut2-G6s*, black, $n = 22$
1272 ganglia) and Snap25-GCaMP6s animals (*Snap25-G6s*, red, $n = 7$ ganglia). No
1273 significant differences were found in vagal responses to intestinal delivery of fat or sugar
1274 between the *Vglut2-G6s* and *Snap25-G6s* genetic drivers (Two-sided Mann–Whitney U-
1275 test, $P = 0.29$ for sugar/nutrient responders, $P = 0.83$ for fat-only responders). All values
1276 are mean \pm s.e.m.

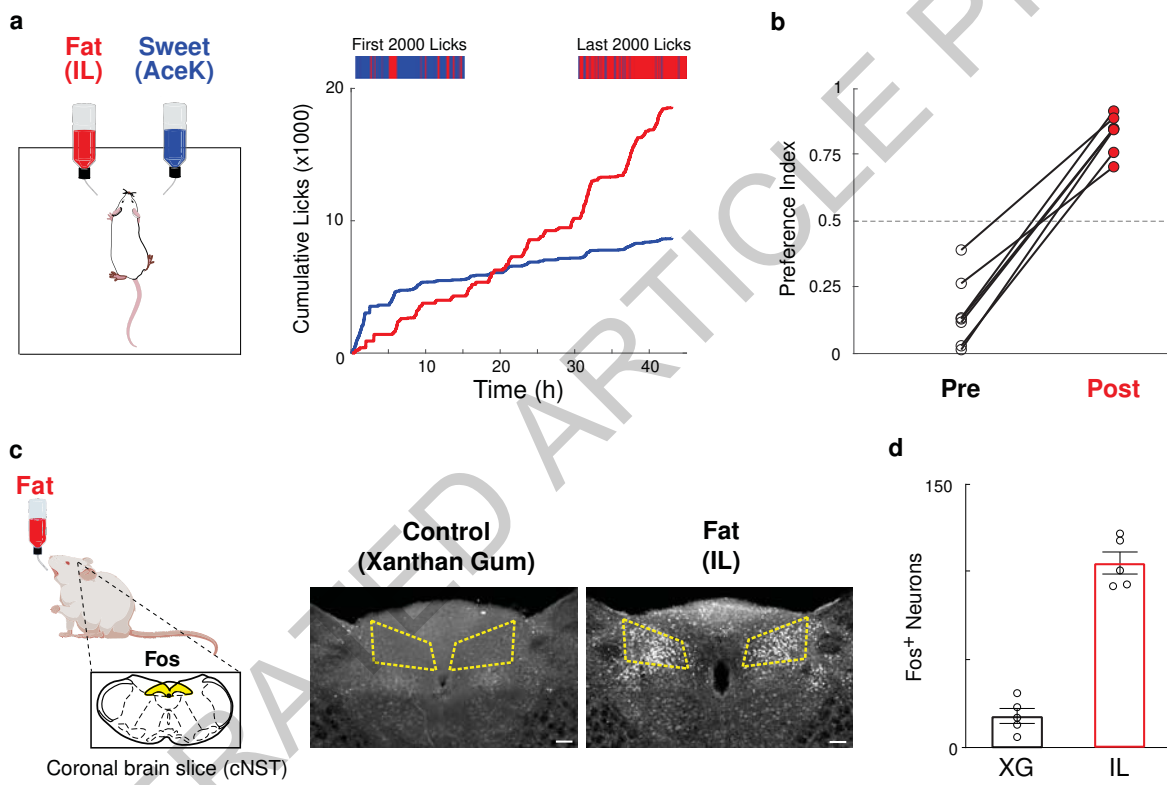
1277

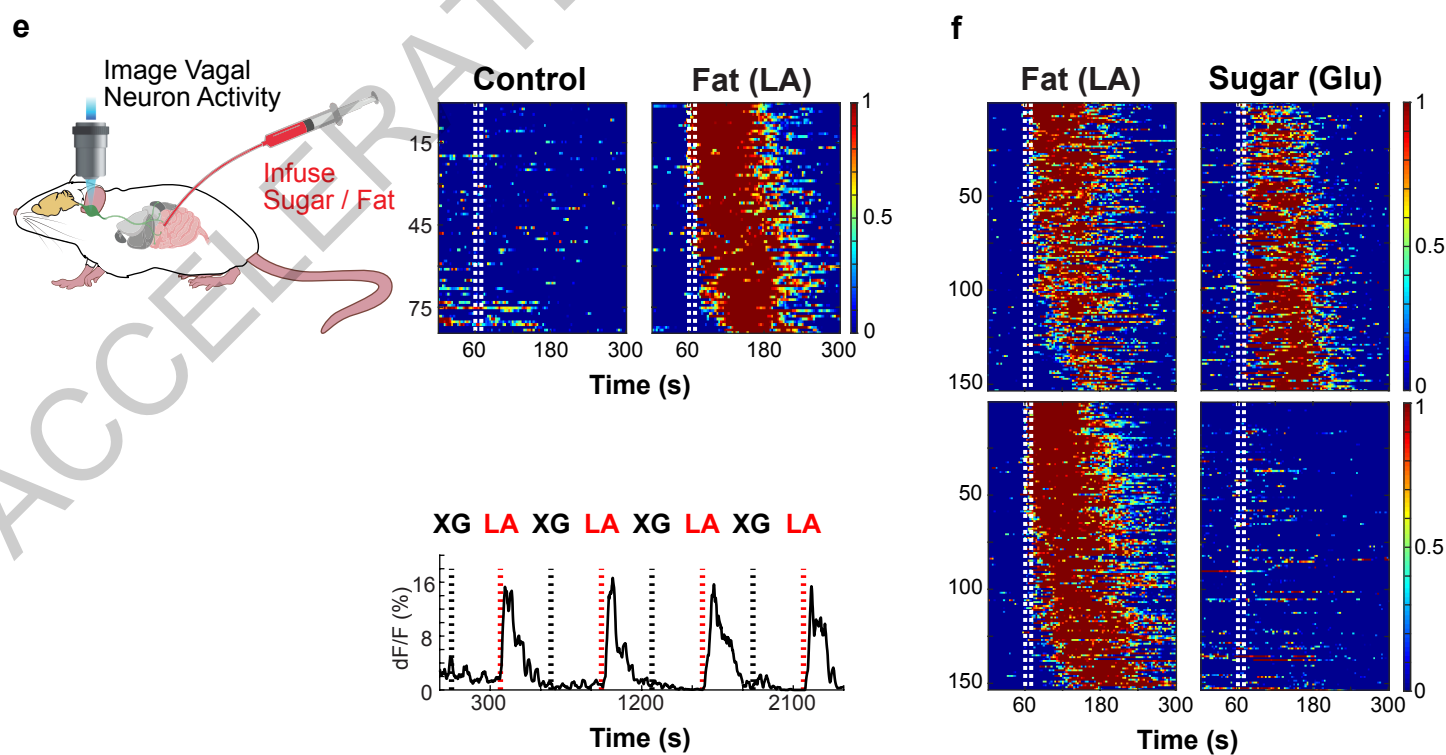
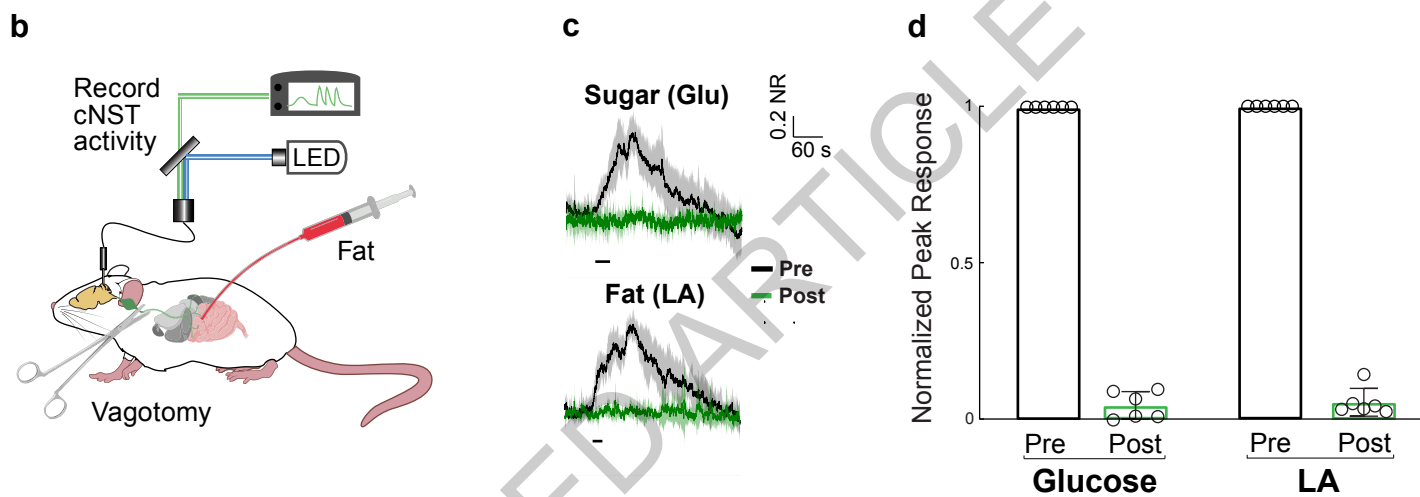
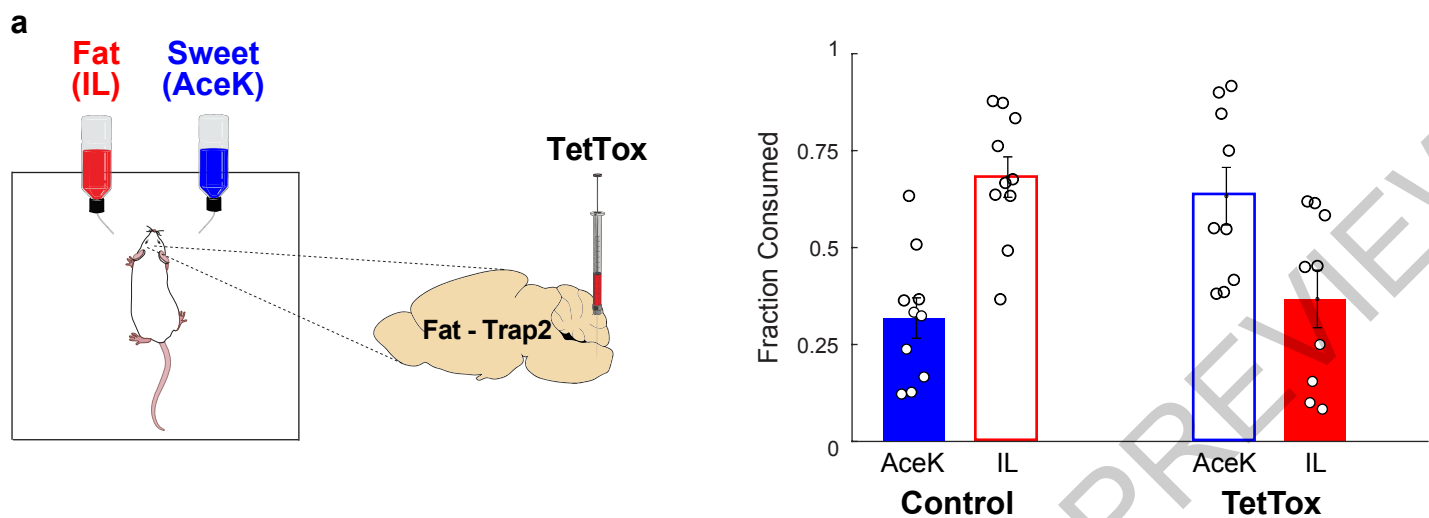
1278 **Extended Data Figure 10: Functional imaging of vagal responses in fat receptor**
1279 **knockouts**

1280 **a-f**, Functional imaging of vagal neurons in response to intestinal delivery of fat
1281 (10% linoleic acid) and sugar (500 mM glucose) in Snap25-GCaMP6s mice harbouring
1282 various combinations of fat receptor deletions (see text for details). Heat maps show
1283 sugar/nutrient responders (top panels), and fat-only responders (bottom panels). **a**,
1284 control ($n = 7$ ganglia); **b**, CD36 KO ($n = 6$ ganglia); **c**, GPR40 KO ($n = 7$ ganglia); **d**,
1285 GPR120 KO ($n = 6$ ganglia); **e**, CD36 & GPR40 double KO ($n = 6$ ganglia); **f**, CD36 &
1286 GPR120 double KO ($n = 8$ ganglia). See Fig. 6c for GPR40 & GPR120 double KO and
1287 triple KO heat maps. **g**, Comparison of vagal responses to intestinal sugar stimuli in all
1288 fat receptor knockouts (see Fig. 6 for fat responses). ANOVA with Tukey's HSD test to
1289 WT ($n = 7$): CD36 KO ($n = 6$ mice), $P = 0.99$; GPR40 KO (R40, $n = 7$ mice), $P = 0.87$;
1290 GPR120 KO (R120, $n = 6$ mice), $P = 0.94$; CD36/GPR40 double KO (CD36/R40, $n = 6$
1291 mice), $P = 0.99$; CD36/GPR120 double KO, (CD36/R120, $n = 8$ mice), $P =$
1292 0.96; GPR40/GPR120 double KO (R40/120, $n = 7$ mice), $P = 0.99$;
1293 CD36/GPR40/GPR120 triple KO (3KO, $n = 6$ mice), $P = 0.99$. Values are mean \pm s.e.m.
1294 **h**, Fat receptor knockout animals that cannot transmit the gut-brain signal
1295 (GPR40/GPR120 double knockouts, and the triple knockout) still exhibit normal innate
1296 attraction to fat stimuli. Shown are brief-access (30 min) two-bottle tests for artificial
1297 sweetener (3 mM AceK) versus water (left panel), and fat (1.5% Intralipid, IL) versus
1298 water (right panel). ANOVA with Tukey's test compared to wild type sweet consumption
1299 ($n = 9$): GPR40/GPR120 double KO (R40/R120): $n = 6$, $P = 0.96$;

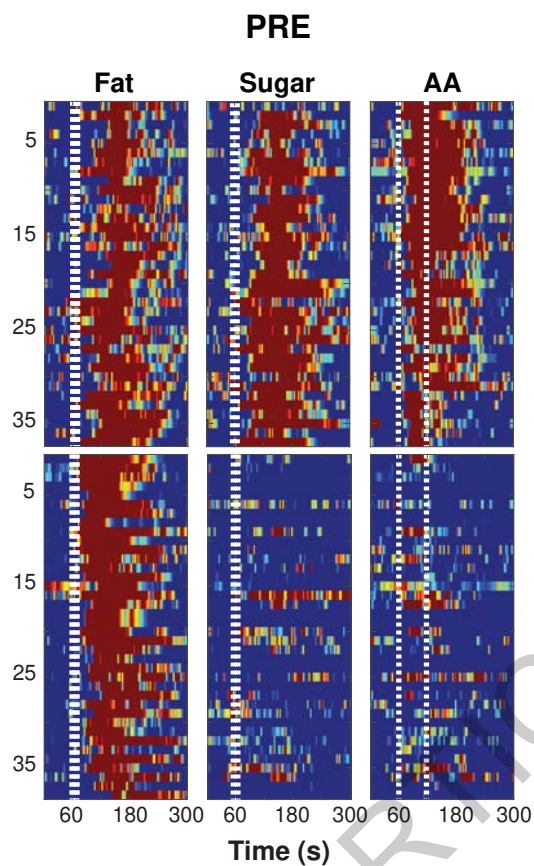
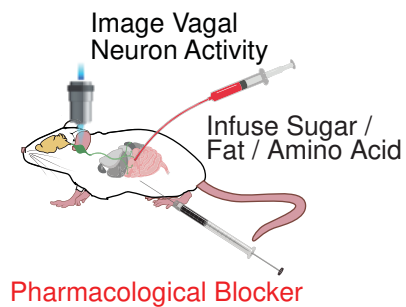
1300 CD36/GPR40/GPR120 triple KO (D36/R40/R120): $n = 5$, $P = 0.26$. ANOVA with Tukey's
1301 test compared to wild type fat consumption, R40/R120: $n = 6$, $P = 0.25$; $n = 5$,
1302 D36/R40/R120: $P = 0.98$. Two-tailed paired t-test. Values are mean \pm s.e.m.

ACCELERATED ARTICLE PREVIEW

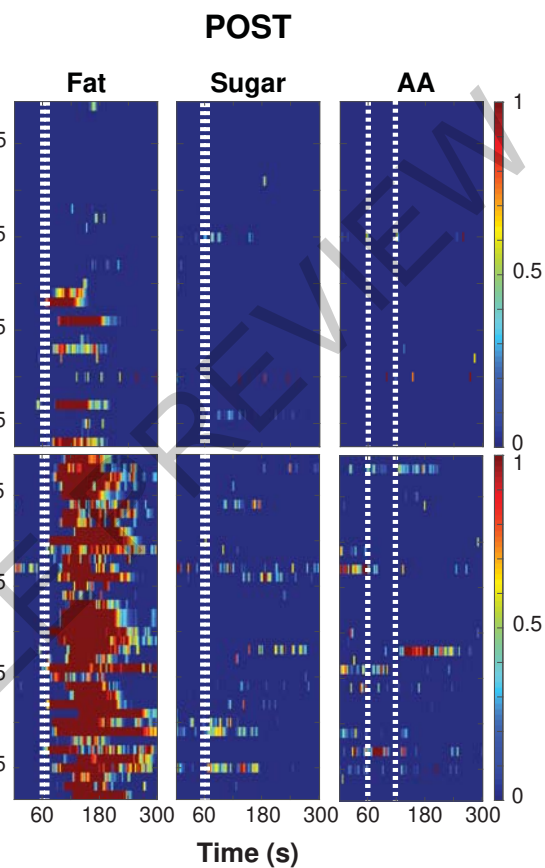




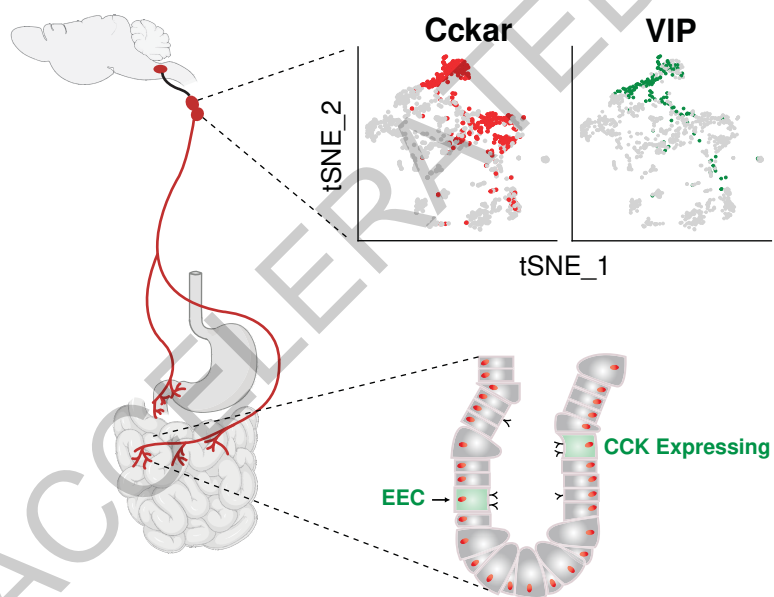
a



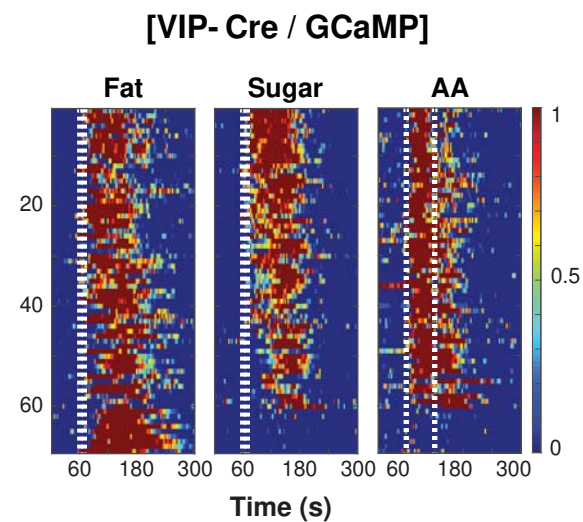
b

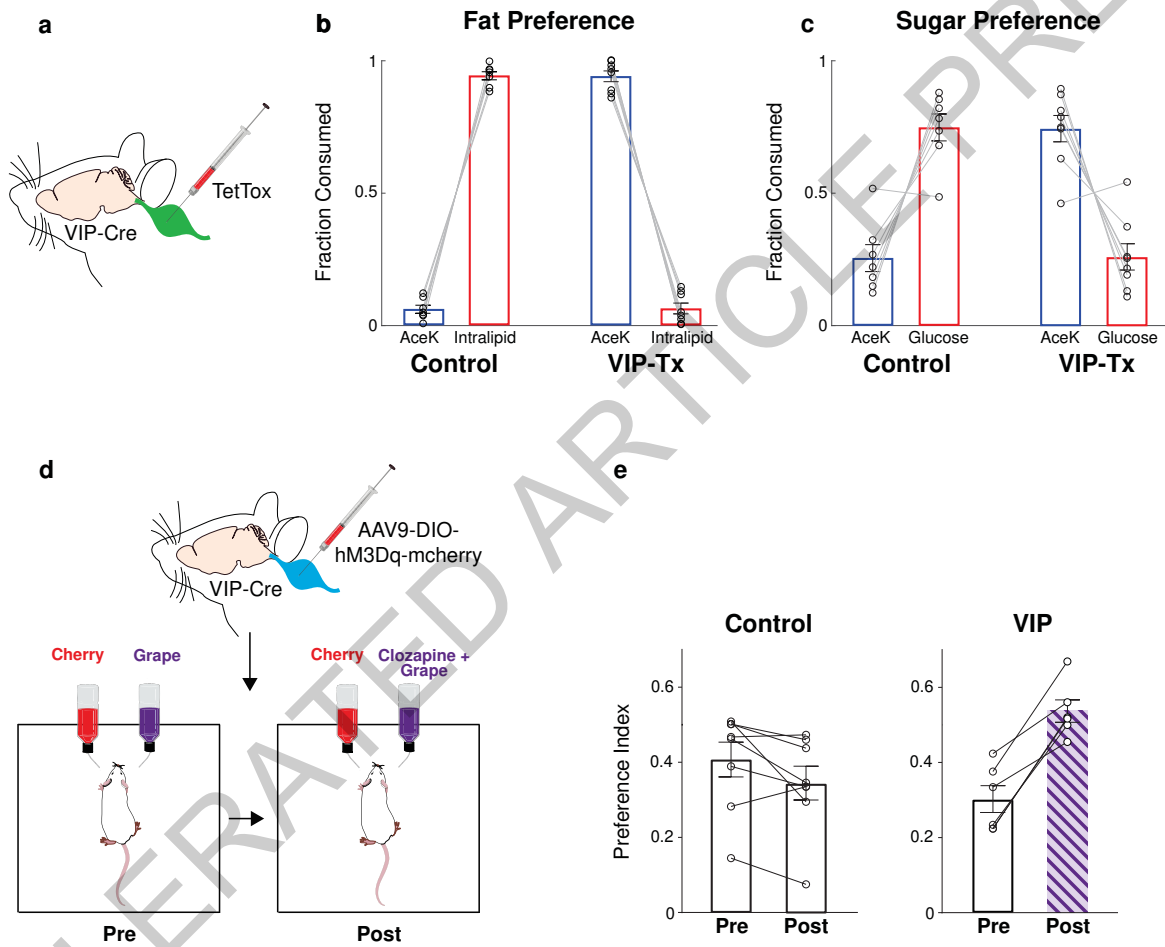


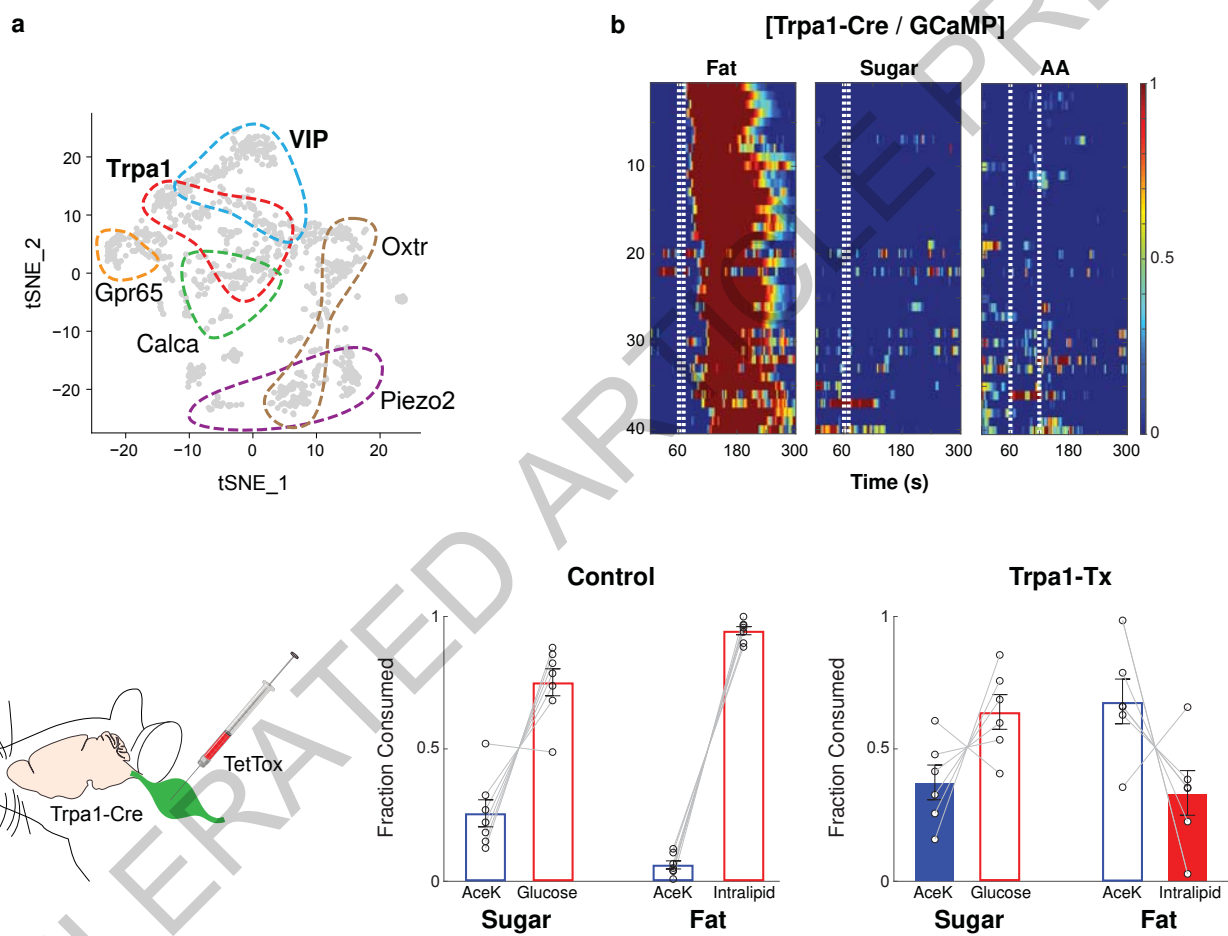
c

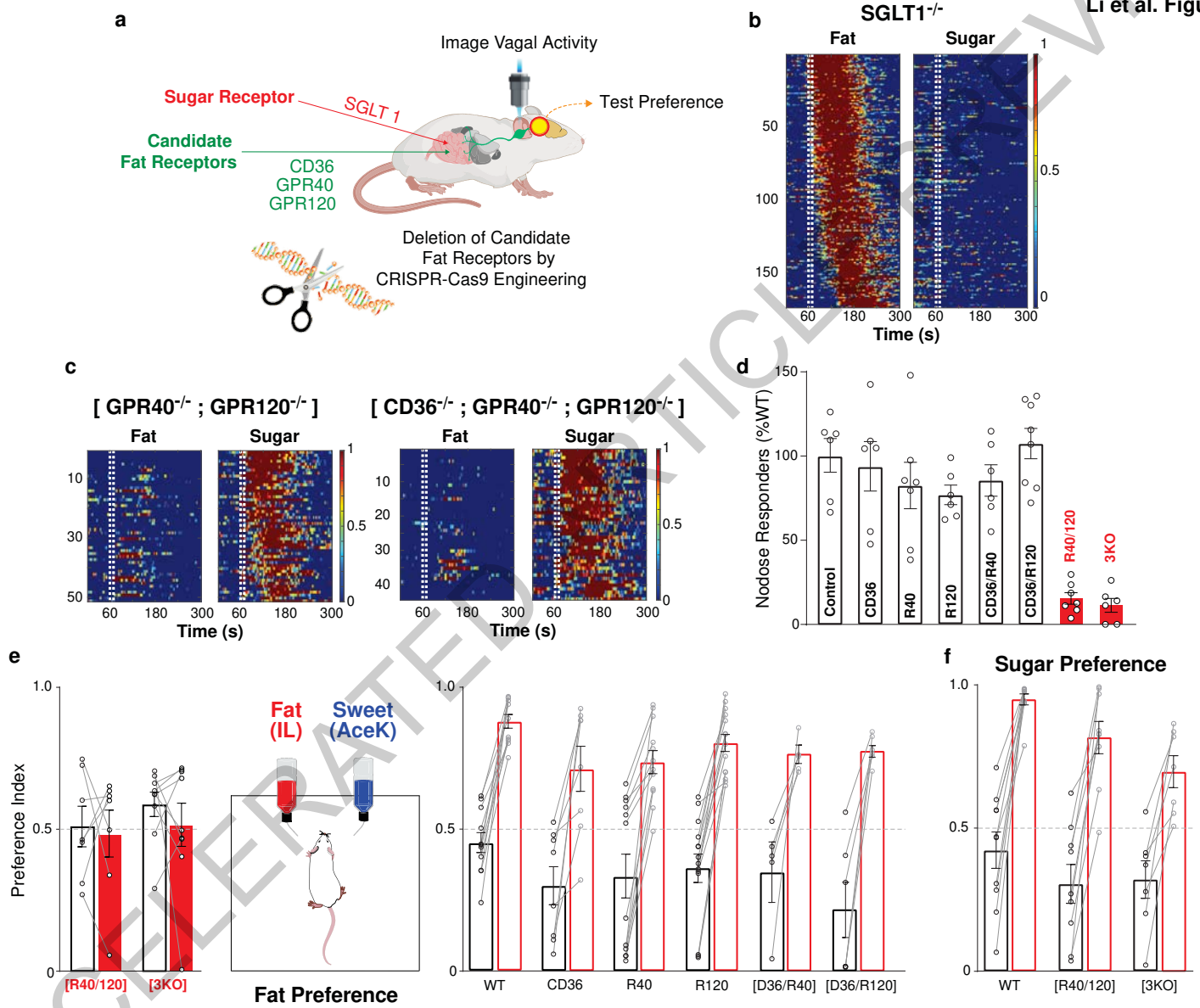


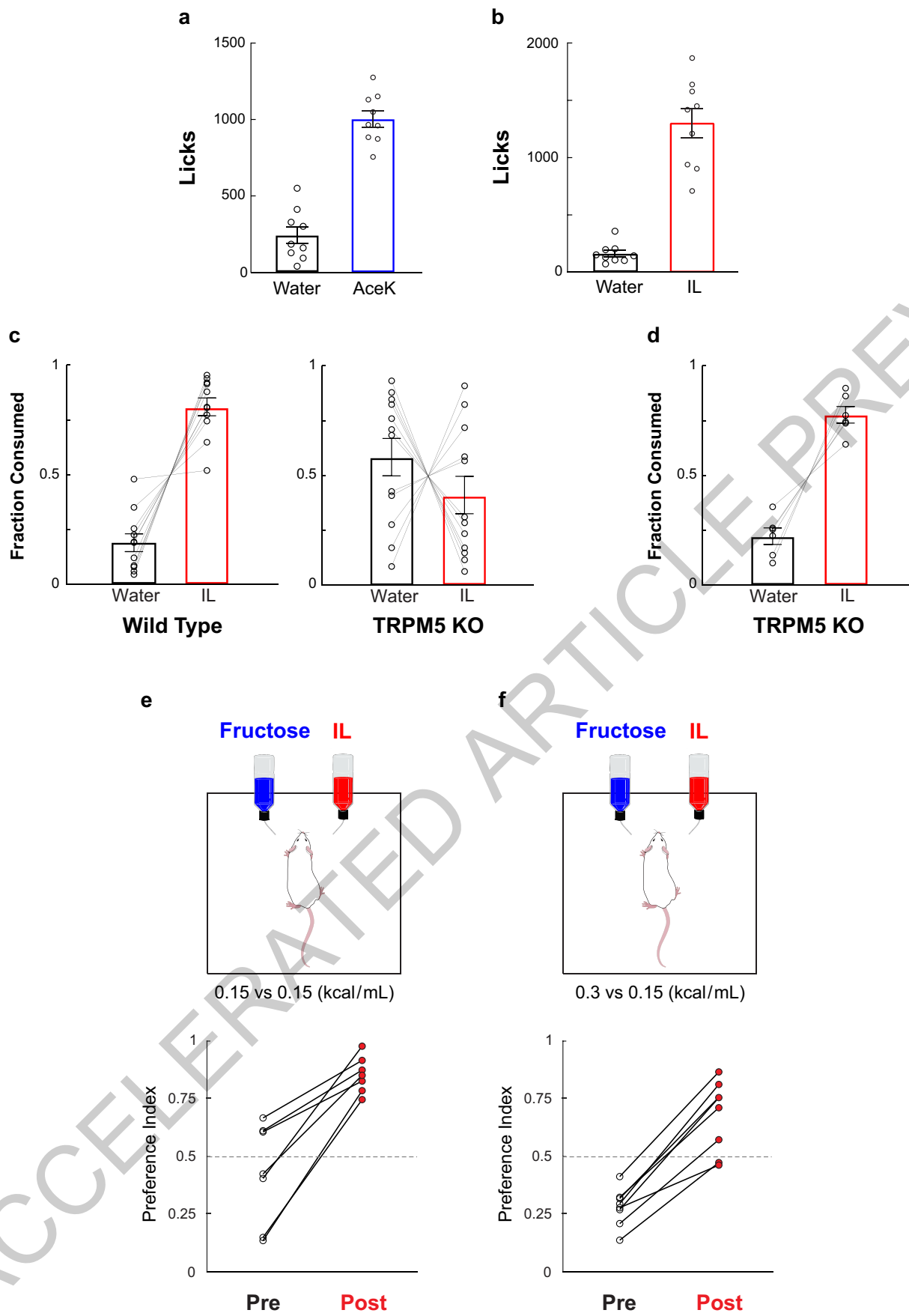
d



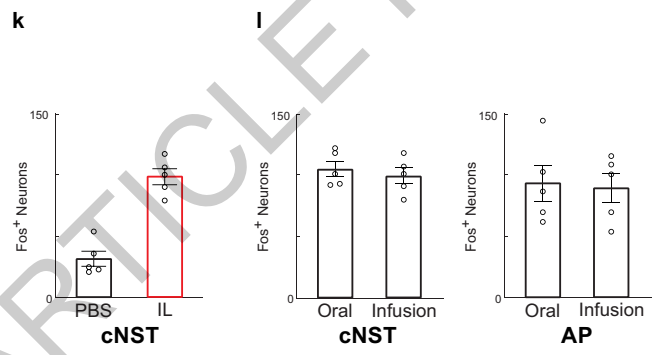
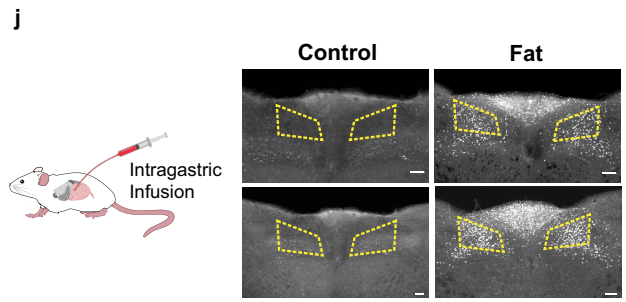
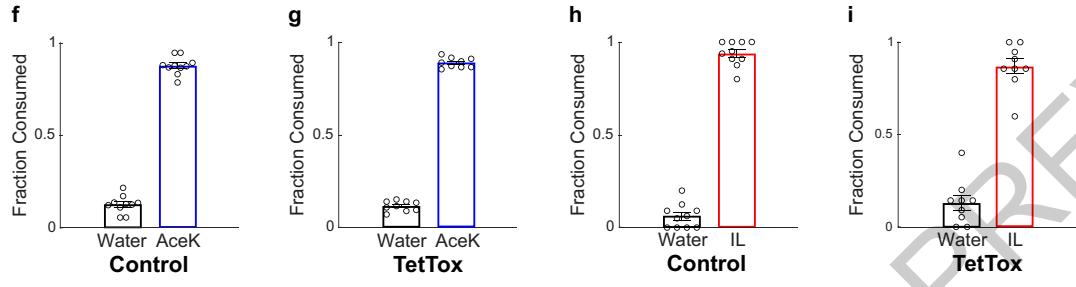
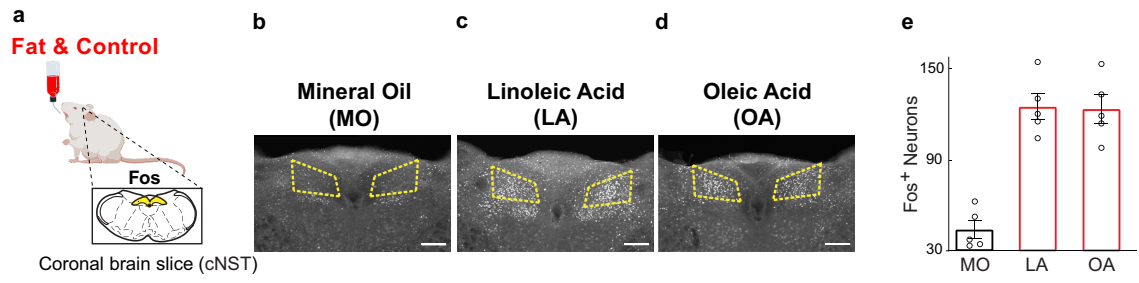






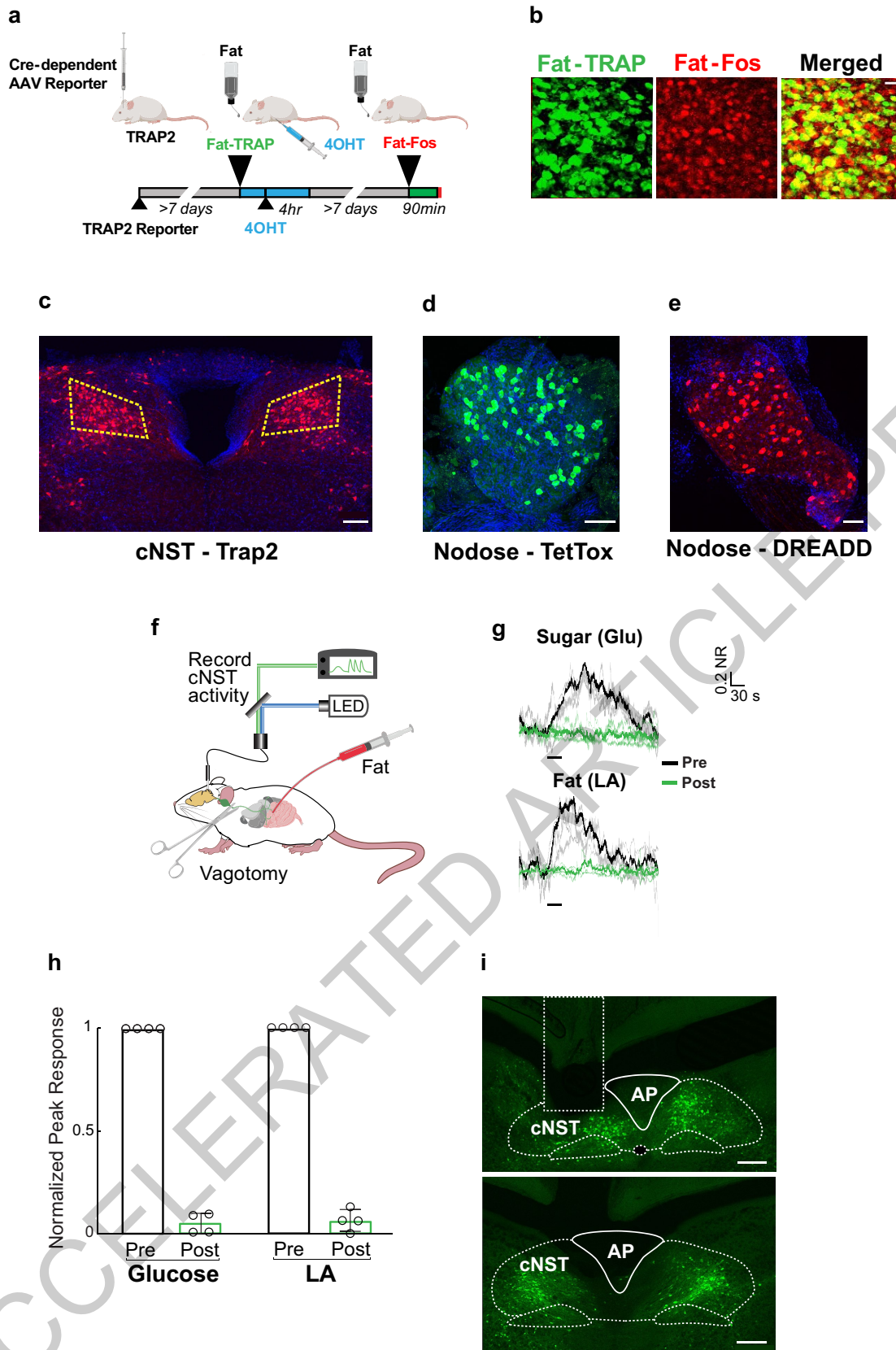


Extended Data Fig. 1

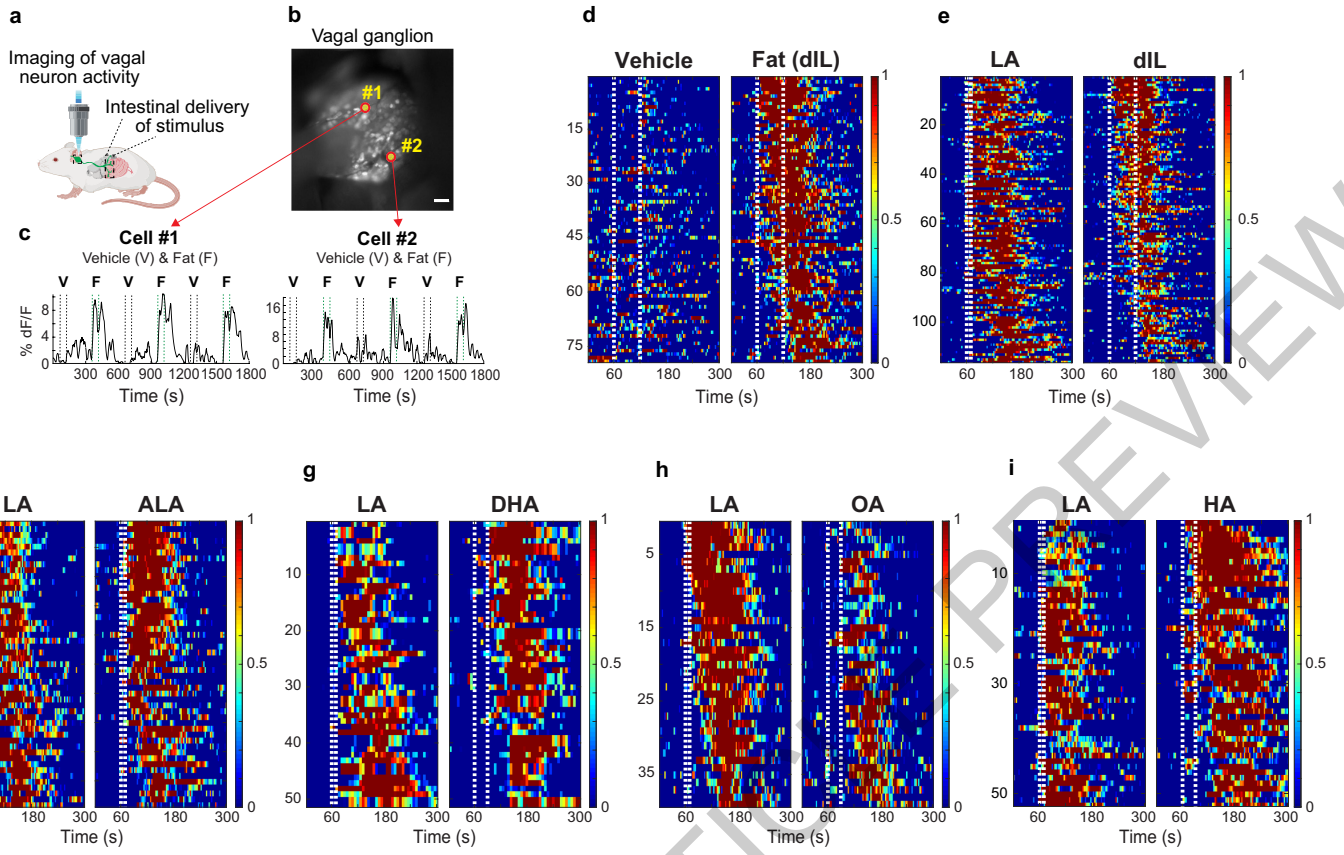


Extended Data Fig. 2

ACCELERATED ARTICLE PREVIEW

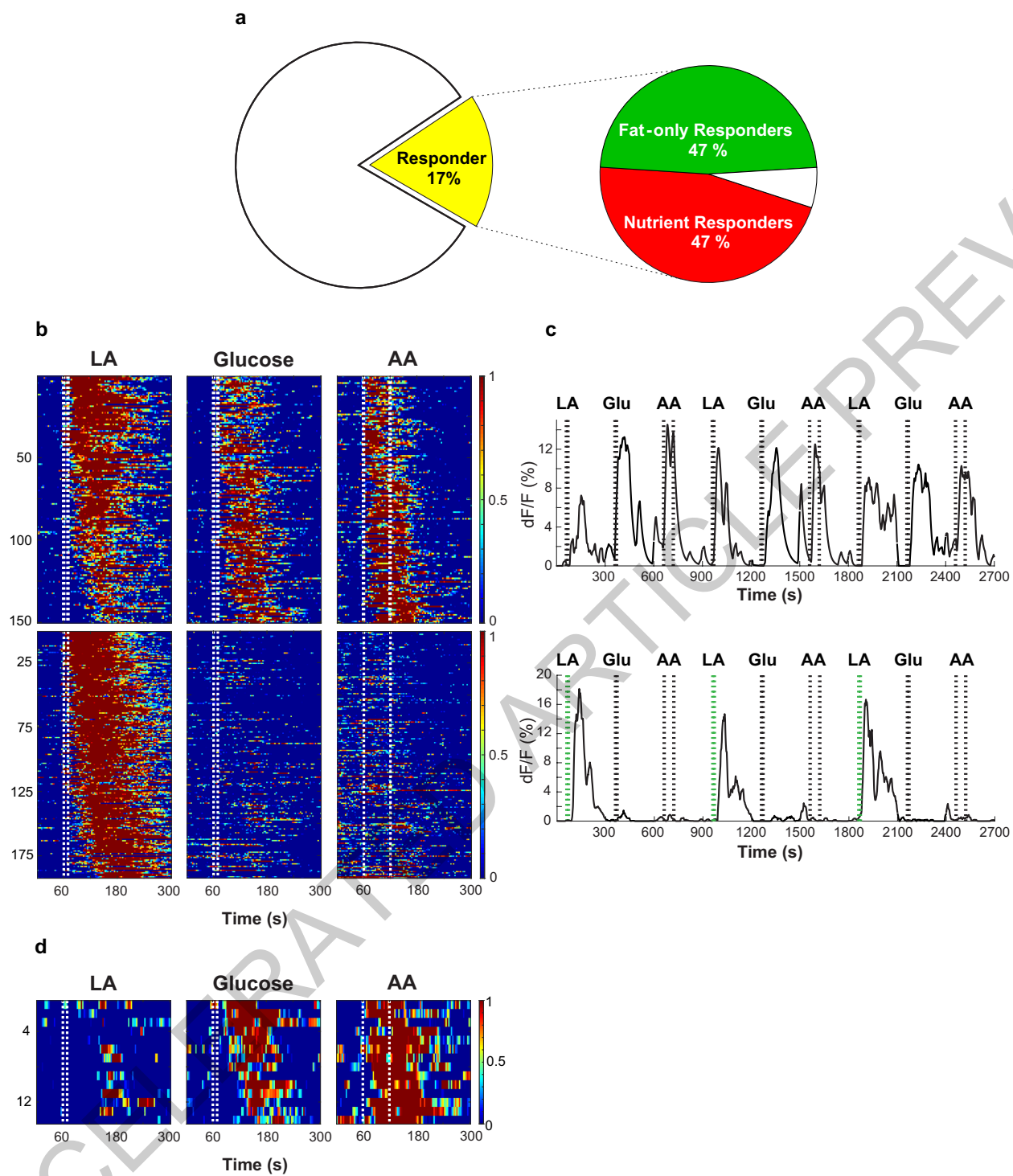


Extended Data Fig. 3

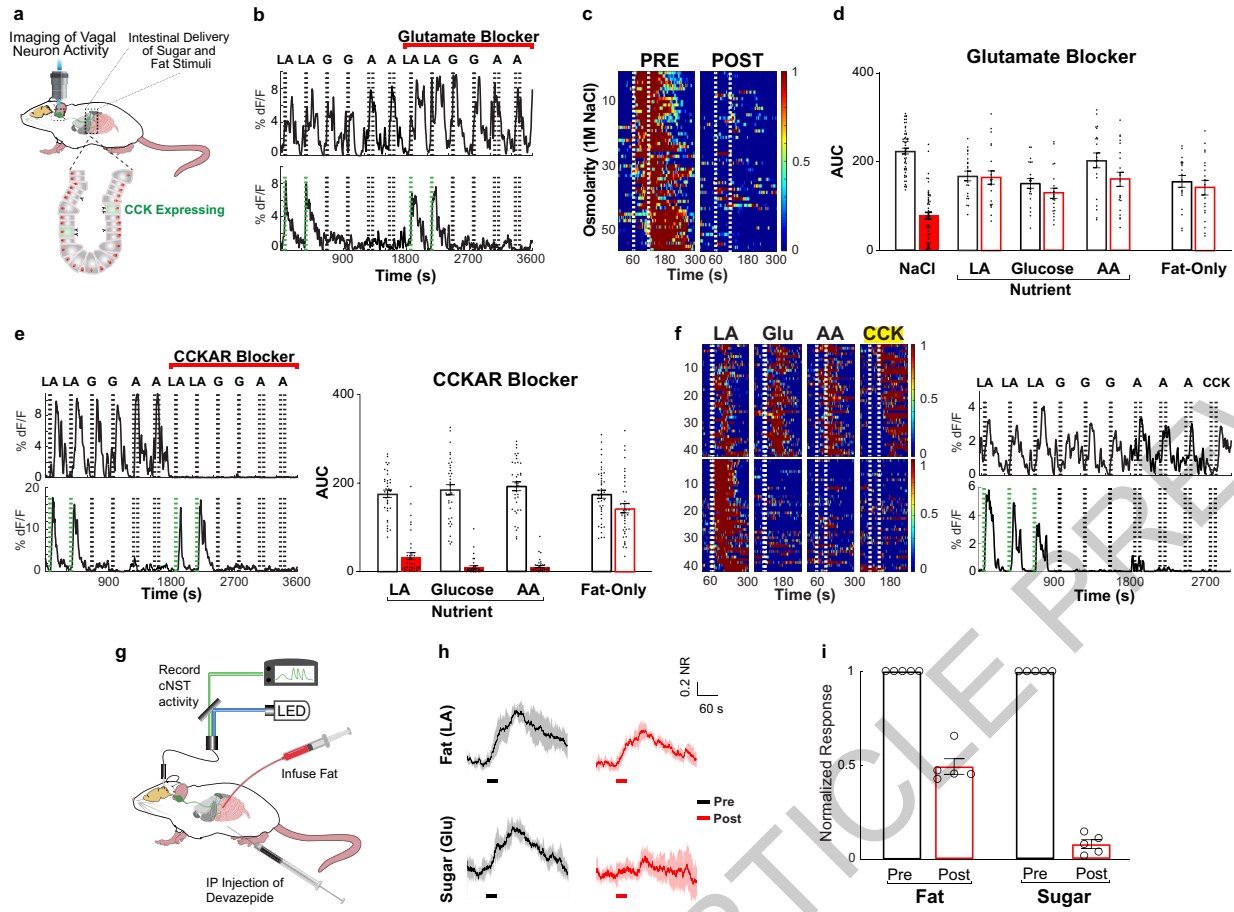


Extended Data Fig. 4

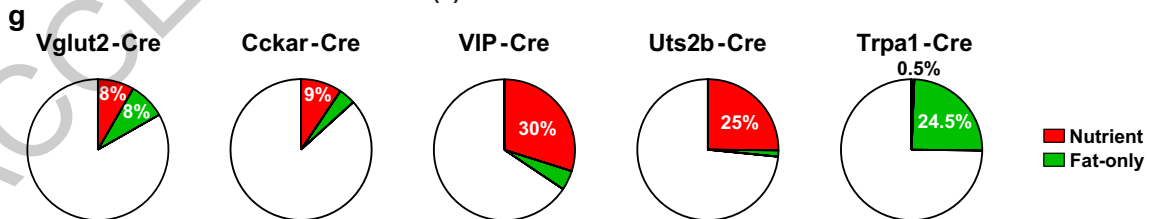
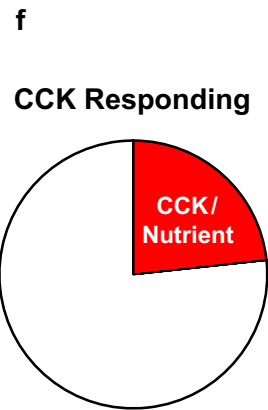
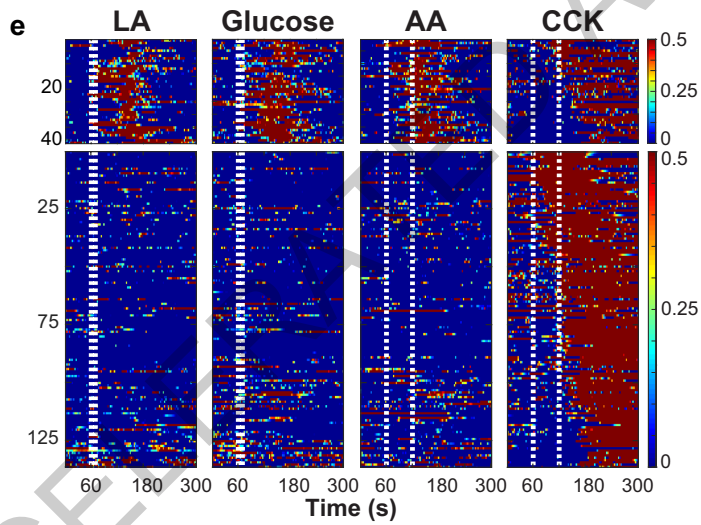
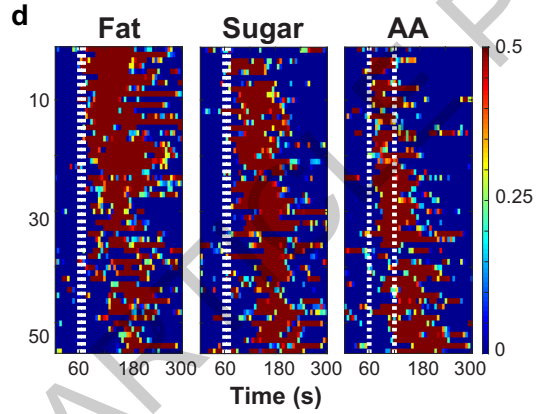
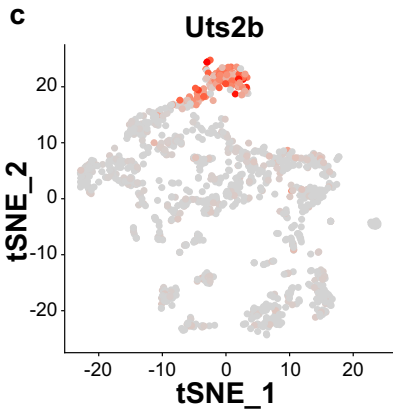
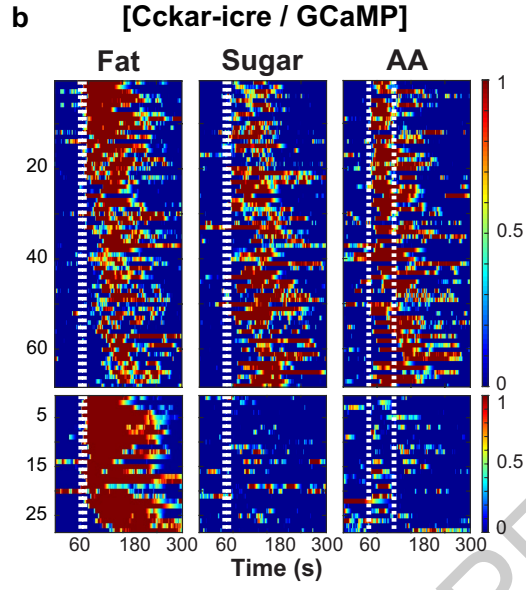
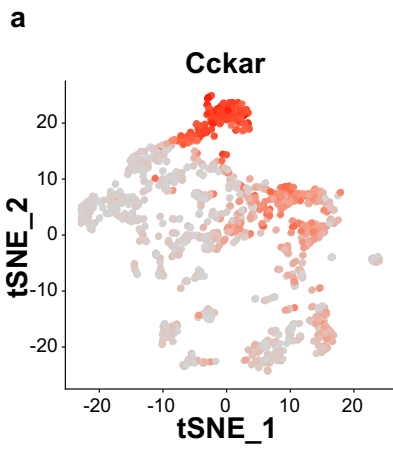
ACCELERATED ARTI...



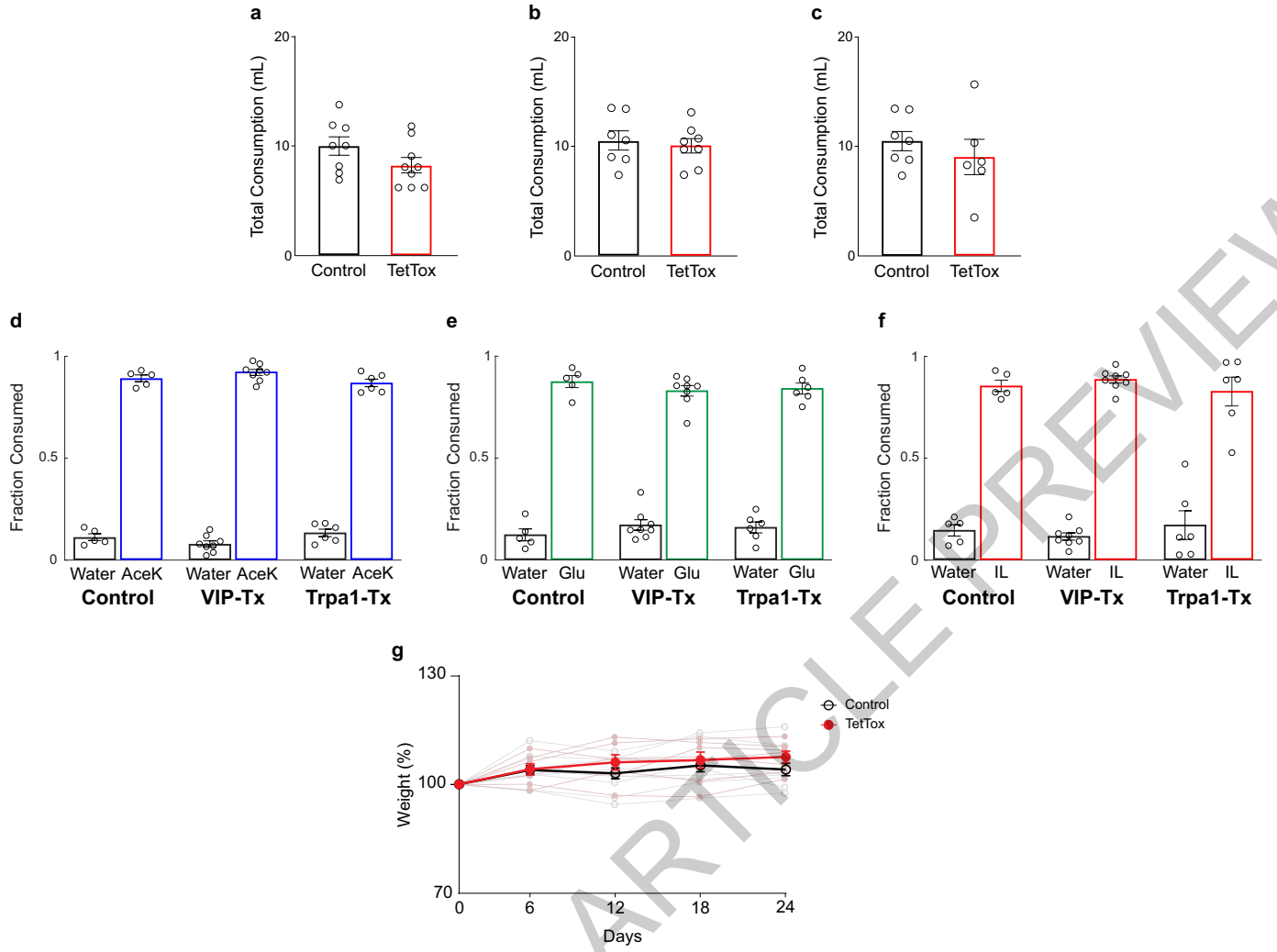
Extended Data Fig. 5



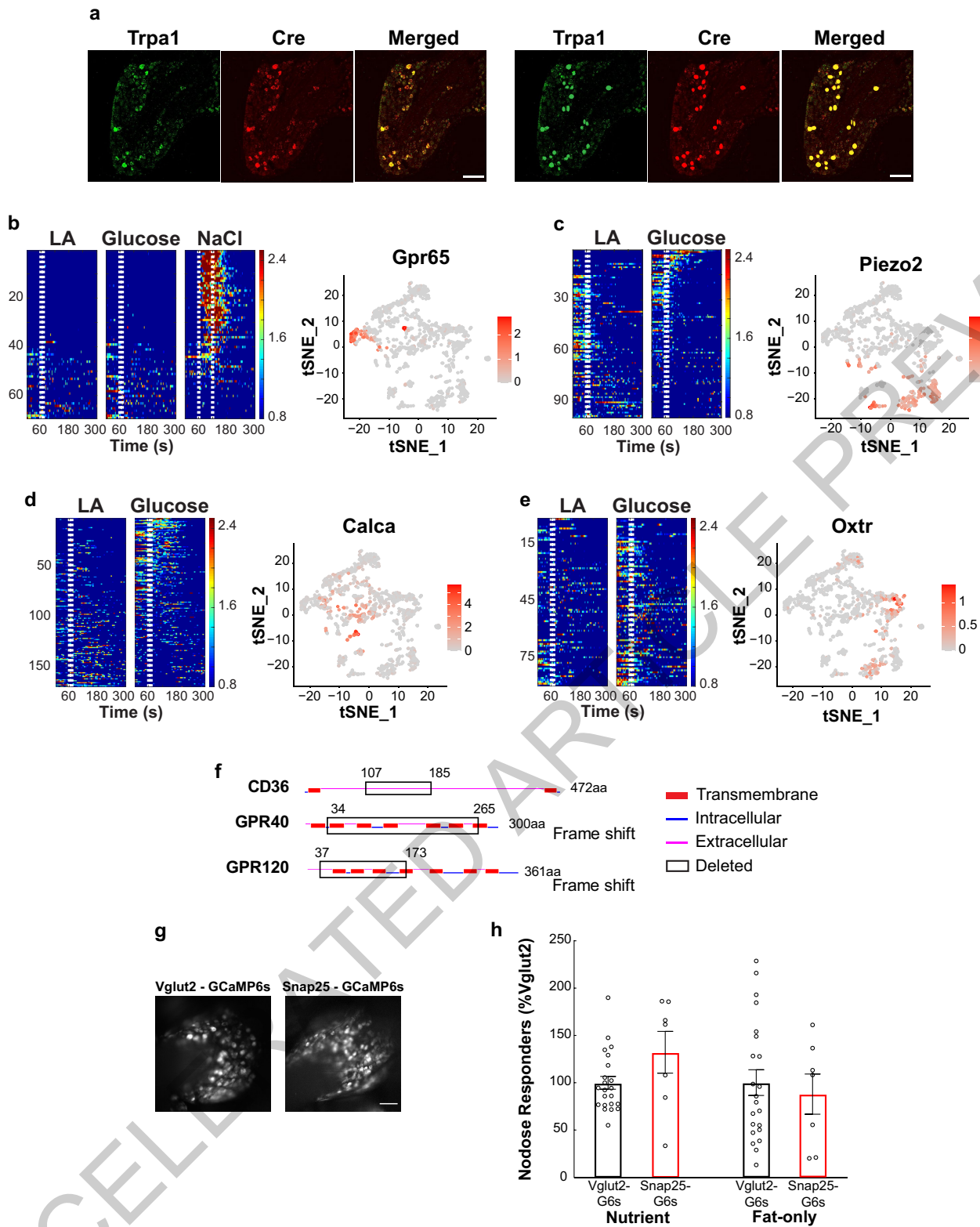
Extended Data Fig. 6



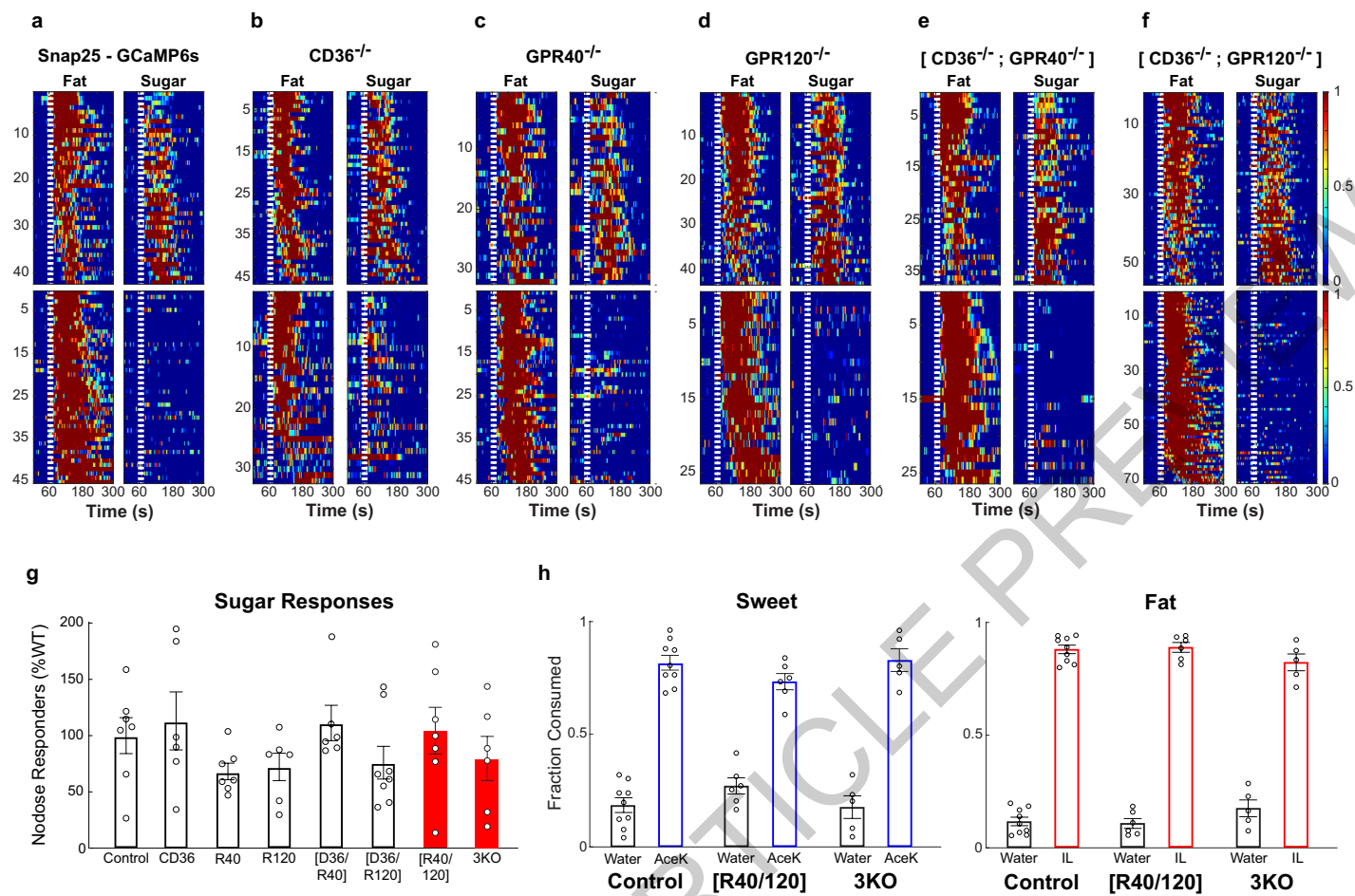
Extended Data Fig. 7



Extended Data Fig. 8



Extended Data Fig. 9



Extended Data Fig. 10

Reporting Summary

Nature Portfolio wishes to improve the reproducibility of the work that we publish. This form provides structure for consistency and transparency in reporting. For further information on Nature Portfolio policies, see our [Editorial Policies](#) and the [Editorial Policy Checklist](#).

Statistics

For all statistical analyses, confirm that the following items are present in the figure legend, table legend, main text, or Methods section.

n/a Confirmed

- The exact sample size (n) for each experimental group/condition, given as a discrete number and unit of measurement
- A statement on whether measurements were taken from distinct samples or whether the same sample was measured repeatedly
- The statistical test(s) used AND whether they are one- or two-sided
Only common tests should be described solely by name; describe more complex techniques in the Methods section.
- A description of all covariates tested
- A description of any assumptions or corrections, such as tests of normality and adjustment for multiple comparisons
- A full description of the statistical parameters including central tendency (e.g. means) or other basic estimates (e.g. regression coefficient) AND variation (e.g. standard deviation) or associated estimates of uncertainty (e.g. confidence intervals)
- For null hypothesis testing, the test statistic (e.g. F , t , r) with confidence intervals, effect sizes, degrees of freedom and P value noted
Give P values as exact values whenever suitable.
- For Bayesian analysis, information on the choice of priors and Markov chain Monte Carlo settings
- For hierarchical and complex designs, identification of the appropriate level for tests and full reporting of outcomes
- Estimates of effect sizes (e.g. Cohen's d , Pearson's r), indicating how they were calculated

Our web collection on [statistics for biologists](#) contains articles on many of the points above.

Software and code

Policy information about [availability of computer code](#)

Data collection Tucker-Davis Technologies Synapse (Version 90-39473P), MicroManager (Version 1.4), Olympus Fluoview (FV10), Arduino IDE (Version 1.8.15), MathWorks Matlab (R2019a, R2019b)

Data analysis MathWorks Matlab (R2019a, R2019b), Fiji (Version 1.53c), GraphPad Prism 8.4.3

For manuscripts utilizing custom algorithms or software that are central to the research but not yet described in published literature, software must be made available to editors and reviewers. We strongly encourage code deposition in a community repository (e.g. GitHub). See the Nature Portfolio [guidelines for submitting code & software](#) for further information.

Data

Policy information about [availability of data](#)

All manuscripts must include a [data availability statement](#). This statement should provide the following information, where applicable:

- Accession codes, unique identifiers, or web links for publicly available datasets
- A description of any restrictions on data availability
- For clinical datasets or third party data, please ensure that the statement adheres to our [policy](#)

All data supporting the findings of this study are available upon request.

Human research participants

Policy information about [studies involving human research participants and Sex and Gender in Research](#).

Reporting on sex and gender

Use the terms *sex* (biological attribute) and *gender* (shaped by social and cultural circumstances) carefully in order to avoid confusing both terms. Indicate if findings apply to only one sex or gender; describe whether sex and gender were considered in study design whether sex and/or gender was determined based on self-reporting or assigned and methods used. Provide in the source data disaggregated sex and gender data where this information has been collected, and consent has been obtained for sharing of individual-level data; provide overall numbers in this Reporting Summary. Please state if this information has not been collected. Report sex- and gender-based analyses where performed, justify reasons for lack of sex- and gender-based analysis.

Population characteristics

Describe the covariate-relevant population characteristics of the human research participants (e.g. age, genotypic information, past and current diagnosis and treatment categories). If you filled out the behavioural & social sciences study design questions and have nothing to add here, write "See above."

Recruitment

Describe how participants were recruited. Outline any potential self-selection bias or other biases that may be present and how these are likely to impact results.

Ethics oversight

Identify the organization(s) that approved the study protocol.

Note that full information on the approval of the study protocol must also be provided in the manuscript.

Field-specific reporting

Please select the one below that is the best fit for your research. If you are not sure, read the appropriate sections before making your selection.

Life sciences Behavioural & social sciences Ecological, evolutionary & environmental sciences

For a reference copy of the document with all sections, see nature.com/documents/nr-reporting-summary-flat.pdf

Life sciences study design

All studies must disclose on these points even when the disclosure is negative.

Sample size

Sample size was determined based similar studies in the literature and our experience. No statistical method was used to determine the sample size prior to the study.

Data exclusions

Animals in which post-hoc histological examination showed that viral targeting or the position of implanted fiber were in the incorrect location were excluded from analysis. This exclusion criteria was predetermined.

Replication

We performed multiple independent experiments as noted in the figure legends. Results were reproducible.

Randomization

Stimuli order was random, otherwise in situations as described in the manuscript where no randomization was used, the stimuli were interspersed and repeated among trials.

Blinding

Investigators were not blinded to group allocation, as data analysis was performed automatically with the same scripts executed for each experimental group.

Reporting for specific materials, systems and methods

We require information from authors about some types of materials, experimental systems and methods used in many studies. Here, indicate whether each material, system or method listed is relevant to your study. If you are not sure if a list item applies to your research, read the appropriate section before selecting a response.

Materials & experimental systems

Methods

n/a	Involvement
<input type="checkbox"/>	<input checked="" type="checkbox"/> Antibodies
<input checked="" type="checkbox"/>	<input type="checkbox"/> Eukaryotic cell lines
<input checked="" type="checkbox"/>	<input type="checkbox"/> Palaeontology and archaeology
<input type="checkbox"/>	<input checked="" type="checkbox"/> Animals and other organisms
<input checked="" type="checkbox"/>	<input type="checkbox"/> Clinical data
<input checked="" type="checkbox"/>	<input type="checkbox"/> Dual use research of concern

n/a	Involvement
<input checked="" type="checkbox"/>	<input type="checkbox"/> ChIP-seq
<input checked="" type="checkbox"/>	<input type="checkbox"/> Flow cytometry
<input checked="" type="checkbox"/>	<input type="checkbox"/> MRI-based neuroimaging

Antibodies

Antibodies used	anti c-Fos (Synaptic Systems, 226004, Guinea Pig, 1:5000),
Validation	antibodies has been validated extensively, e.g. by immuno-staining on mouse brain sections (Song, et al. Science advances, 52: eaat 3210, (2019)).

Animals and other research organisms

Policy information about [studies involving animals](#); [ARRIVE guidelines](#) recommended for reporting animal research, and [Sex and Gender in Research](#)

Laboratory animals	Adult animals 6-24 weeks of age and from both genders were used in experiments. C57BL/6J (JAX 000664), TRAP2 (JAX 030323), TRPM5 KO (JAX 013068), Ai96 (JAX 028866), Ai162 (JAX 031562), VGlut2-IRES-Cre (JAX 028863), Gpr65-IRES-Cre (JAX 029282), Vip-IRES-Cre (JAX 010908); Uts2b-Cre (JAX 035452); Piezo2-Cre (JAX 027719); Oxtr-Cre (JAX 031303); Calca-Cre (JAX 033168); Snap25-2A-GCaMP6s (JAX 025111), Penk-IRES2-Cre (JAX 025112).
Wild animals	No wild animals were used.
Reporting on sex	Animals of both sexes were used in the behavioral and imaging studies, without bias.
Field-collected samples	No field-collected samples were used.
Ethics oversight	All procedures were carried out in accordance with the US National Institutes of Health (NIH) guidelines for the care and use of laboratory animals, and were approved by the Institutional Animal Care and Use Committee at Columbia University.

Note that full information on the approval of the study protocol must also be provided in the manuscript.